Review Article
Clustering of X-Ray-Selected AGN

N. Cappelluti,[1, 2] V. Allevato,[3] and A. Finoguenov[2, 4]

[1] Osservatorio Astronomico di Bologna, INAF, Via Ranzani 1, 40127 Bologna, Italy
[2] University of Maryland, Baltimore County, 1000 Hilltop Circle, Baltimore, MD 21250, USA
[3] Max-Planck-Institut für Plasmaphysik and Excellence Cluster Universe, Boltzmannstrasse 2, 85748 Garching, Germany
[4] Max-Planck-Institute für Extraterrestrische Physik, Giessenbachstrasse 1, 85748 Garching, Germany

Correspondence should be addressed to N. Cappelluti, nico.cappelluti@oabo.inaf.it

The study of the angular and spatial structure of the X-ray sky has been under investigation since the times of the *Einstein* X-ray Observatory. This topic has fascinated more than two generations of scientists and slowly unveiled an unexpected scenario regarding the consequences of the angular and spatial distribution of X-ray sources. It was first established from the clustering of sources making the CXB that the source spatial distribution resembles that of optical QSO. It then became evident that the distribution of X-ray AGN in the Universe was strongly reflecting that of Dark Matter. In particular, one of the key results is that X-ray AGNs are hosted by dark matter halos of mass similar to that of galaxy groups. This result, together with model predictions, has lead to the hypothesis that galaxy mergers may constitute the main AGN-triggering mechanism. However, detailed analysis of observational data, acquired with modern telescopes, and the use of the new halo occupation formalism has revealed that the triggering of an AGN could also be attributed to phenomena-like tidal disruption or disk instability and to galaxy evolution. This paper reviews results from 1988 to 2011 in the field of X-ray-selected AGN clustering.

1. Introduction

After about 50 years from the opening of the X-ray window on the Universe with the discovery of Sco-X1 and the Cosmic X-ray background (CXB, [1]), our knowledge of high-energy processes in the Universe has dramatically improved. One of the leading mechanisms for the production of X-ray in the Universe is accretion onto compact objects. For this reason, the study of astrophysical X-ray sources is a powerful tool for studying matter under the effects of extreme gravity. As the efficiency of converting matter into energy in accretion processes is proportional to the "compactness" of the object (i.e., $\propto$ M/R), it is clear that the strongest sources powered by accretion are super-massive black holes (SMBH). It also became a cornerstone of astrophysics that every galaxy with a bulge-like component hosts a SMBH at its centre and that the BH mass and the bulge velocity dispersion are strictly related [2]. It is also believed that black holes reach those high masses via one or more phases of intense accretion activity and therefore shining as active galactic nuclei (AGN). It is

believed that an AGN basically shines mostly from the power emitted by a thin, viscous, accretion disk orbiting the central SMBH Shakura and Sunyaev [3]. Such a disk produces a high amount of X-rays both from its hot inner regions (as far as the soft X-ray emission is concerned) and from a nonthermal source which is supposed to be the primary source of X-rays (both soft and hard).

Since its discovery, the nature of the CXB has been strongly debated, but soon the community converged into interpreting most of the CXB as the integrated emission of AGN across the cosmic time. While the discrete nature of the CXB has been proposed [4] and rapidly unveiled by experiments like *Einstein* [1] and ROSAT (see, e.g., [5]), little cosmological information has been obtained from samples of AGN because of the scarce number of detected sources in the X-ray band. Structure formation models and numerical simulations have shown that structures in the Universe have undergone a hierarchical growth starting from the denser peaks in the primordial Gaussian matter distribution. The large-scale structures (LSS) of the Universe

are gravitationally dominated by dark matter (DM), and we can consider it as the responsible and one of the main drivers of the Cosmological structures evolution. Dark matter is believed to clump in large-scale halos (DMH Navarro, [6]) which are populated by galaxies. Thus, galaxies can be considered as tracers of the DM distribution in the Universe, and the study of their spatial clustering led us to a most comprehensive view of the LSS. On the other hand AGN/Quasar, as phase of the galactic evolution, is a quite rare phenomenon in the Universe as their space density of these objects is about 1/100–1/1000 lower than that of galaxies. This means that AGN/Quasar survey requires large field of view and/or deep exposure to provide statistically significant samples.

The study of their clustering and its evolution is a powerful tool to understand, from a statistical point of view, what kind of environment is more likely to host AGN. This is not just an academic question, but this is strictly related to the mechanism of AGN activation. We know that one of the candidate mechanisms for triggering an AGN is galaxy merger (see, e.g., [7–10]). The probability of such an event is definitely dependent on the environment inhabited by the host galaxy. Even if the mean distance between galaxies is relatively small, in high-density (mass) environments, they have a high velocity dispersion, and, therefore, the likelihood of a major merger is very low. On the contrary, in the field, the likelihood of galaxy mergers is low because of the large average distance between galaxies. The most favorable place to detect a merger is therefore a moderately low-density (mass) environment like a group (see, e.g., [11]).

In fact, merger-driven models (see, e.g., [7]) accurately predict the observed large-scale clustering of quasars as a function of redshift up to $z{\sim}4$. The clustering is precisely that predicted for small group halos in which major mergers of gas-rich galaxies should proceed most efficiently. Thus, it is well established empirically and with theoretical predictions that quasar clustering traces a characteristic host halo mass $\sim 4 \times 10^{12} h^{-1} M_{\odot}$, supporting the scenario in which major mergers dominate the bright quasar populations.

In addition, other phenomena like secular processes may become dominant at lower luminosities as suggested by Milosavljević et al. [12]; Hopkins et al. [13]; Hopkins and Henquist [9]. Low-luminosity AGN could be triggered in more common nonmerger events, like stochastic encounters of the black holes and molecular clouds, tidal disruption, or disk instability. This leads to the expectation of a characteristic transition to merger-induced fueling around the traditional quasar-Seyfert luminosity division (growth of BH masses above/below $\sim 10^7 M_{\odot}$). However, the triggering mechanism of the SMBH growth must be compliant with M_{BH}-σ relation that links the growth of the SMBH with growth of the bulge of the host galaxy [2].

As shown in Hopkins et al. [8], the predicted large-scale bias of quasars triggered by secular processes is, at all redshifts, lower than the bias estimated for quasars fueled by major mergers. This implies that low-luminosity Seyfert galaxies live in DMHs that never reach the characteristic mass associated with small group scales.

On the other hand, the majority of the results on the clustering of X-ray-selected AGN suggest a picture where moderate-luminosity AGN live in massive DMHs ($12.5 < \log M_{DMH} [h^{-1} M_{\odot}] < 13.5$) up to $z \sim 2$, that is, X-ray-selected AGN samples appear to cluster more strongly than bright quasars. The reason for this is not completely clear, but several studies argued that these large bias and DMH masses could suggest a different AGN-triggering mechanism respect to bright quasars characterized by galaxy merger-induced fueling.

This paper reviews results of clustering of X-ray-selected AGN from the first *Einstein* to the most recent *Chandra* and XMM-*Newton* surveys. We give a detailed description of the methods used in this kind of analysis from simple power-law to halo models. In addition, we discuss the results of X-ray AGN clustering in the framework of AGN evolution and triggering. We adopt a ΛCDM cosmology with $\Omega_{\Lambda} = 0.7$, $\Omega_m = 0.3$, $H_0 = 100 h^{-1}$ km/s/Mpc with h = 0.7 and $\sigma_8 = 0.8$ ([14], WMAP-7).

2. Previous Measures of X-Ray Clustering Amplitude

As far as the X-ray source clustering results are concerned, the development of the field has always been driven by the performance of the telescopes. In particular, while first results studied the angular distribution of the unresolved CXB under the assumption that Quasars were its main contributors, recent *Chandra* and XMM-*Newton* surveys sample clustering of AGN with a precision comparable to that achievable with redshift galaxy surveys.

In the following section, we will use the following convention for reporting results of clustering analysis in the case of power-law representation of the auto(cross)-correlation function: if the clustering is measured in the angular space, we will use

$$w(\theta) = \left(\frac{\theta}{\theta_0}\right)^{1-\gamma}, \tag{1}$$

where θ_0 is the angular correlation length. If the measurements have been performed in the real (redshift) space this becomes

$$\xi(r) = \left(\frac{r}{r_0}\right)^{-\gamma}, \qquad \left(\xi(s) = \left(\frac{s}{s_0}\right)^{-\gamma}, \quad \text{in } z-\text{space}\right), \tag{2}$$

where γ is the 3D correlation slope and r_0 or s_0 are the correlation lengths. Barcons and Fabian [15] measured with *Einstein* a clustering signal of the CXB on scales $\leq 5'$ corresponding to an angular correlation length $\theta_0 \sim 4'$. They have shown the importance of studying the angular structure of the CXB by pointing out that a large fraction of the CXB could have been attributed to sources with a redshift distribution similar to optical QSOs. In addition, the first prediction was not consistent with the hypothesis that the CXB was also partly produced by a diffuse hot intergalactic medium (IGM) component. It was also proposed that these

sources were actually clustered on comoving scales of the order of $\sim$10 h^{-1} Mpc.

Carrera and Barcons [16], Georgantopoulos et al. [17], and Soltan and Hasinger [18] observed that the CXB was highly isotropic on scales of the order of 2°–25°. The first attempt of measuring the clustering of X-ray-selected AGN was performed by Boyle and Mo [19] that measured a barely significant signal by using a sample of 183 EMSS sources, mostly local AGN ($z < 0.2$). These evidences have brought the attention to the study of the clustering of the CXB down to the arcminute scale. The first significant upward turn for the measurement of AGN clustering in the X-ray band has been brought to light by ROSAT. By using a set of ROSAT-PSPC pointing on an area of $\sim 40 \deg^2$, Vikhlinin and Forman [20] measured, for the first time, an angular correlation signal of faint (ROSAT) X-ray sources on scales <10$'$. By using the Limber equation (see Appendix B and [21]) they have deprojected their angular correlation function into a real-space correlation function and found that, under the assumption that the redshift distribution of the sources was the same as that of optical QSOs, the spatial correlation length was in the range 6–10 h^{-1} Mpc. With such a result, they confirmed the hypothesis that the CXB was mostly produced by sources with a redshift distribution comparable to that of optically selected QSO, though with almost double source density. By using the results of Vikhlinin and Forman [20] and Akylas et al. [22] (who obtained similar results), Barcons et al. [23] have shown for the first time that X-ray-selected AGNs are highly biased tracers of the underlying LSS at $z < 1$ by showing a redshift evolving bias factor as large as $b \sim 2$.

However, it is worth to consider that the deprojection of the angular correlation function into a 3D correlation relies on several assumptions, like the model-dependent expected redshift distribution, which may lead to a biased estimate of the real-space clustering. It is, however, worth noticing that angular correlation can be very useful to provide a first overview in the early phase of surveys, when optical identifications are not available, especially sampling new part of the parameter space of sources, like that is, new unexplored luminosity/flux limits and therefore source classes. Detailed physical models are, however, much better investigated by more sophisticated techniques as shown in the following parts.

The first firm detection of 3D spatial clustering of X-ray-selected AGN has been claimed by Mullis et al. [24] by using data of the ROSAT-NEP survey. They detected on an area of $\sim$81 deg^2 a 3σ significant signal in the redshift space autocorrelation function of soft X-ray-selected sources at $\langle z \rangle \sim$0.22. They have shown that, at that redshift AGN cluster with a typical correlation length, $r_0 = 7.4 \pm 1.9$ h^{-1} Mpc. Their results suggest that the population of AGN in such a sample is consistent with an unbiased population with respect to the underlying matter. Their result suggested that, at that redshift, AGNs were hosted in DMHs of mass of the order of $10^{13} h^{-1} M_\odot$.

With the development of *Chandra* and XMM-*Newton* surveys and thanks to the high source surface densities (i.e., >400–1000 deg^{-2}), our capabilities in tracing the LSS

have dramatically increased. One of the first evidences that AGNs are highly correlated with the underlying LSS has been pointed out by Cappi et al. [25] and Cappelluti et al. [26] and references therein, who showed that, around massive high-z galaxy clusters, the source surface density of *Chandra* point sources is significantly, up to two times, higher than that of the background. More recently, Koulouridis and Plionis [27] showed that, although the X-ray source surface density of AGN around galaxy clusters is larger than in the background, the amplitude of their overdensities is about 4 times lower than that of galaxies in the same fields. This has been interpreted as a clear indication of an environmental influence on the AGN activity. Silverman et al. [10] in the COSMOS field and Koss et al. [28] in the *Swift*-BAT all-sky survey have shown that the AGN fraction in galaxy pairs is higher relative to isolated galaxies of similar stellar mass providing an additional evidence of the influence of the environment on AGN activity.

Chandra and XMM-*Newton* performed several blanck sky extragalactic surveys, and most of them dedicated part of their efforts in the study of the LSS traced by AGN to unveil their coevolution. Basilakos et al. [29, 30] by using data of the XMM-*Newton* 2dF-survey have measured an unexpected high correlation length both in the angular ($\theta_0 \sim 10''$) and, by projection, in the real space ($r_0 \sim 16$ h^{-1} Mpc). Such a high correlation length has been detected in this field only, thus one can explain such a measurement as a statistical fluctuation. With the same technique, Gandhi et al. [31] obtained a marginal 2-3σ detection of angular clustering in the XMM-LSS survey and obtained $\theta_0 = 6.3(42) \pm 3(^{+7}_{-13})$ in the 0.5–2 (2–10) keV bands and a slope $\gamma \sim 2.2$. Puccetti et al. [32] measured the clustering of X-ray sources in the XMM-*Newton* ELAIS-S1 survey in the soft and hard energy bands with a sample of 448 sources. They obtained $\theta_0 = 5.2 \pm 3.8\,4''$ and $\theta_0 = 12.8 \pm 7.8\,4''$ in the two bands, respectively. These measurements have been deprojected with the Limber's inversion in the real space and obtained $r_0 = 9.8$–12.8 h^{-1} Mpc and $r_0 = 13.4$–17.9 h^{-1} Mpc in the two bands, respectively.

In the *Chandra* era, Gilli et al. [33] measured the real space autocorrelation function of point sources in the CDFS-CDFN. They have measured, in the CDFS, $r_0 = 8.6 \pm 1.2$ h^{-1} Mpc at $z = 0.73$, while, in the CDFN, they obtained $r_0 = 4.2 \pm 0.4$ h^{-1} Mpc. The discrepancy of these measurements has been explained with variance introduced by the relatively small field of view and the consequent random sampling of LSSs in the field. In the CLASXS survey, Yang et al. [34] obtained a measurement of the clustering at $z = 0.94$ with $r_0 = 8.1^{+1.2}_{-2.2}$ h^{-1} Mpc which proposes that AGNs are hosted by DMH of mass of $10^{12.1}$ h^{-1} $M_\odot$ (see Section 3). In addition, they proposed that AGN clustering evolves with luminosity and they found that the bias factor evolves with the redshift. Such a behavior is similar to that found in optically selected quasars. The XMM-*Newton* [35–37] and *Chandra* [38, 39] survey of the COSMOS field have provided a leap forward to the field of X-ray AGN clustering by surveying a 2 deg^2 field of view. The key of the success of this project is a redshift survey *zCOSMOS* [40] performed simultaneously with the X-ray

survey, together with observations in more than 30 energy bands from radio to X-ray that allowed to measure either the spectroscopic or the photometric redshift of every source. In the X-ray band, the survey covers $2 \deg^2$ with XMM-*Newton* with a depth of ~60 ks with the addition of a central $0.9 \deg^2$ observed by *Chandra* with ~150 ks exposure. The first sample of ~1500 X-ray sources [36] has been used by Miyaji et al. [41] to determine their angular correlation function, without knowing their distance, and just assuming a theoretical redshift distribution for the purpose of Limber's deprojection. Significant positive signals have been detected in the 0.5–2 band, in the angular range of $0.5'$–$24'$, while the positive signals were at the ~2σ and 3σ levels in the 2–4.5 and 4.5–10 keV bands, respectively. With power-law fits to the ACFs without the integral constraint term, they have found correlation lengths of $\theta_0 = 1.9 \pm 0.3''$, $0.8^{+0.5}_{-0.4}$, and $6 \pm 2''$ for the three bands, respectively, for a fixed slope $\gamma = 1.8$. The inferred comoving correlation lengths were $r_0 = 9.8 \pm 0.7$, $5.8^{+1.4}_{-1.7}$, and $12 \pm 2 \, h^{-1}$ Mpc at the effective redshifts of $z = 1.1$, 0.9, and 0.6, respectively. Comparing the inferred rms fluctuations of the spatial distribution of AGNs $\sigma_{8,\text{AGN}}$ (see Appendix D) with those of the underlying dark matter, the bias parameters of the X-ray source clustering at these effective redshifts were found in the range $b = 1.5$–4. Such a result leads to the conclusion that the typical mass of the DMH hosting an AGN is of the order $M_{\text{DMH}} \sim 10^{13} \, M_\odot \, h^{-1}$. Similar results have been found by Ebrero et al. [42] using the angular correlation function of 30000 X-ray sources in the AXIS survey. In the XMM-LSS survey, Elyiv et al. [43] measured the clustering of ~5000 AGN and computed via Limber's deprojection the obtained $r_0 = 7.2 \pm 0.8$ Mpc/h and $r_0 = 10.1 \pm 0.8$ Mpc/h and $\gamma \sim 2$ in the 0.5–2 keV and 2–10 keV energy bands, respectively. In the XMM-COSMOS field, Gilli et al. [44] measured the clustering of 562 X-ray selected and spectroscopically confirmed AGN. They have obtained that the correlation length of these source, $r_0 = 8.6 \pm 0.5 \, h^{-1}$ Mpc, and slope of $\gamma = 1.88 \pm 0.07$. They also found that, if source in redshift spikes removed, the correlation length decreases to about 5-6 h^{-1} Mpc. Even if not conclusively, they also showed that narrow-line AGN and broad-line AGN cluster in the same way, indicating that both classes of sources share the same environment, an argument in favor of the unified AGN model which predicts that obscuration, and therefore the Type-I/Type II dichotomy is simply a geometrical problem. However, it is worth noticing that such a procedure may artificially reduce the clustering signal and the effects of such a cut in the sample may lead to an unreliable estimate of the clustering signal.

Even if the results of Gilli et al. [44] provide a quite complete overview of the environments of the AGN in the COSMOS field, Allevato et al. [45] analyzed the same field by using the halo model formalism (see Section 3). Their results show that AGNs selected in the X-ray band are more biased than the more luminous optically selected QSO. This observation significantly deviates from the prediction of models of merger-driven AGN activity [13, 46], indicating that other mechanisms like disk/bar instability of tidal disruptions may trigger an AGN. They also found that Type

1 AGN are more biased than Type 2 AGNs up to redshift of ~1.5.

In the Böotes field, Hickox et al. [47] explored the connection between different classes of AGN and the evolution of their host galaxies, by deriving host galaxy properties, clustering, and Eddington ratios of AGN selected in the radio, X-ray, and infrared (IR) wavebands from the wide-field ($9 \deg^2$) Böotes survey. They noticed that radio and X-ray AGNs reside in relatively large DMHs ($M_{\text{DMH}} \sim 3 \times 10^{13}$ and $10^{13} \, M_\odot \, h^{-1}$, resp.) and are found in galaxies with red and green colors. In contrast, IR AGNs are in less luminous galaxies, have higher Eddington ratios, and reside in halos with $M_{\text{DMH}} < 10^{12} \, M_\odot \, h^{-1}$.

On the same line, Coil et al. [48] measured the clustering of nonquasar X-ray active galactic nuclei at $z = 0.7$–1.4 in the AEGIS field. Using the cross-correlation of Chandra-selected AGN with 5000 DEEP2 galaxies, they measured a correlation length of $r_0 = 5.95 \pm 0.90 \, h^{-1}$ Mpc and slope $\gamma = 1.66 \pm 0.22$. They also concluded that X-ray AGNs have a similar clustering amplitude as red, quiescent, and "green" transition galaxies at $z \sim 1$ and are significantly more clustered than blue, star-forming galaxies. In addition, they proposed a "sequence" of X-ray AGN clustering, where its strength is primarily determined by the host galaxy color; AGNs in red host galaxies are significantly more clustered than AGNs in blue host galaxies, with a relative bias that is similar to that of red to blue DEEP2 galaxies. They did not observe any dependence of clustering on optical brightness, X-ray luminosity, or hardness ratio. In addition, they obtained evidence that galaxies hosting X-ray AGN are more likely to reside in groups and more massive DMHs than galaxies of the same color and luminosity without an X-ray AGN. Allevato et al. [45], Coil et al. [48] and Mountrichas and Georgakakis [49] concluded that DEEP2 X-ray AGN at $z \sim 1$ are more clustered than optically selected quasars (with a 2.6σ significance) and therefore may reside in more massive DMHs. In an evolutionary picture, their results are consistent with galaxies undergoing a quasar phase while in the blue cloud before settling on the red sequence with a lower-luminosity X-ray AGN, if they are similar objects at different evolutionary stages [47]. At lower redshift, Krumpe et al. [50] confirmed the results of Coil et al. [48]. Various recent works have presented indications and/or evidences, of varying significance, regarding a correlation between the X-ray Luminosity and the AGN clustering amplitude, based either on the spatial [34, 44, 48, 50–52] or the angular [53] correlation function.

Note that luminosity-dependent clustering is one of the key features of merger-triggered AGN activity and is one of the prime motivations for AGN clustering analyses. Low L_X AGNs have been found to cluster in a similar way as blue star forming galaxies while high L_X AGN cluster like red passive galaxies. Such a result has been confirmed by Cappelluti et al. [51] using the Swift-BAT all-sky survey at $z \sim 0$. They detected both a L_X dependence of AGN clustering amplitude and a larger clustering of Type I AGN than that of Type II AGN. Krumpe et al. [50, 52] confirm the weak dependence of the clustering strength on AGN X-ray luminosity at a 2σ level for $z < 0.5$.

Table 1: Cappelluti, Allevato, and Finoguenov.

Survey	Band keV	N_{obj}	z	θ_0 arcsec	r_0 h^{-1} Mpc	γ	$b(z)^a$	Log(M_{DMH})^b $M/(M_\odot h)$
EMSS	0.5–2	183	<0.2	X	<10	X	X	X
RASS	0.1–2.4	2158	1–1.5	~10	<10	1.7 ± 0.3	X	X
RASS	0.1–2.4	2096	0.1	~3.7	6.0 ± 1.6	1.9 ± 0.31	X	X
ROSAT-NEP	0.1–2.4	220	0.22	X	$7.5^{+2.7}_{-4.2}$	$1.85^{+1.90}_{-0.80}$	$1.83^{+1.88}_{-0.61}$	$13.51^{+0.91}_{-0.79}$
AXIS[1]	0.5–2	31288	0.96	22.9 ± 2.0	6.54 ± 0.12	1.12 ± 0.04	2.48 ± 0.07	$13.20^{+0.11}_{-0.12}$
AXIS[1]	2–10	9188	0.94	$29.2^{+5.1}_{-5.7}$	9.9 ± 2.4	$2.33^{+0.10}_{-0.11}$	2.38 ± 0.51	$13.14^{+0.28}_{-0.41}$
AXIS[1]	5–10	1259	0.77	$40.9^{+19.6}_{-29.3}$	5.1 ± 4.1	$1.47^{+0.43}_{-0.57}$	2.14 ± 1.88	$13.17^{+0.84}_{-2.44}$
ELAIS-S1	0.5–2	392	0.4	5.2 ± 3.8	$9.8^{+2.7}_{-4.3}$	1.8	X	X
ELAIS-S1	2–10	205	0.4	12.8 ± 7.8	$13.4^{+2.7}_{-4.3}$	1.8	X	X
CDFS	0.5–2	97	0.84	X	8.6 ± 1.2	1.33 ± 0.11	$2.64^{+0.29}_{-0.30}$	$13.41^{+0.55}_{-0.18}$
CDFN[2]	0.5–2	164	0.96	X	4.2 ± 0.4	1.42 ± 0.07	$1.87^{+0.14}_{-0.16}$	$12.73^{+0.12}_{-0.17}$
XMM-2dF[3]	0.5–2	432	1.2	10.8 ± 1.9	~16	1.8	1.9–2.7	12.5–13.1
XMM-LSS	0.5–2	1130	0.7	6.3 ± 3	6 ± 3	2.2 ± 0.2	X	X
XMM-LSS	2–10	413	0.7	4.2^{+7}_{-13}	6 ± 3	$3.1^{+1.1}_{-0.5}$	X	X
CLASXS	0.5–8	233	1.2	X	$8.1^{+1.2}_{-2.2}$	2.1 ± 0.5	$3.58^{+2.49}_{-1.38}$	$12.86^{+0.61}_{-0.16}$
CDFN[4]	0.5–8	252	0.8	X	$5.8^{+1.0}_{-1.5}$	$1.38^{+0.12}_{-0.14}$	$1.77^{+0.80}_{-0.15}$	$13.53^{+0.63}_{-0.71}$
XMM-COSMOS[5]	0.5–2	1037	1.1	2.9 ± 0.6	11.8 ± 1.1,	1.8	3.7 ± 0.3	13.6 ± 0.1
XMM-COSMOS[5]	2–4.5	545	0.9	$1.2^{+1.1}_{-0.9}$	$6.9^{+2.2}_{-3.1}$,	1.8	$2.5^{+0.7}_{-1.0}$	$13.3^{+0.3}_{-0.7}$
XMM-COSMOS[5]	4.5–10	151	0.6	$6.5^{+3.0}_{-2.7}$	$12.7^{+2.3}_{-2.7}$	1.8	$3.8^{+0.6}_{-0.8}$	13.9 ± 0.2
XMM-COSMOS[6]	0.5–2	538	0.98	X	$8.65^{+0.41}_{-0.48}$	$1.88^{+0.06}_{-0.07}$	3.08 ± 0.14	$13.51^{+0.05}_{-0.07}$
XMM-COSMOS[7]	0.5–2	593	1.21	X	$7.12^{+0.28}_{-0.18}$	$1.81^{+0.04}_{-0.03}$	2.71 ± 0.14	$13.10^{+0.06}_{-0.07}$
SWIFT-BAT	15–55	199	0.045	X	$5.56^{+0.49}_{-0.43}$	$1.64^{+0.07}_{-0.08}$	$1.21^{+0.06}_{-0.07}$	$13.15^{+0.09}_{-0.13}$
AEGIS	0.5–2	113	0.9	X	5.95 ± 0.90	1.66 ± 0.22	$1.97^{+0.26}_{-0.25}$	$13.0^{+0.1}_{-0.4}$
AGES	0.5–2	362	0.51	X	4.5 ± 0.6	1.6 ± 0.1	$1.35^{+0.06}_{-0.07}$	$12.60^{+0.1}_{-0.1}$
ROSAT + SDSS	0.1–2.4	1552	0.27	X	$4.28^{+0.44}_{-0.54}$	$1.67^{+0.13}_{-0.12}$	$1.11^{+0.10}_{-0.12}$	$12.58^{+0.20}_{-0.33}$
XMM-LSS	0.5–2	4360	1.1	3.2 ± 0.5	7.2 ± 0.8	1.93 ± 0.03	2.7 ± 0.3	13.2 ± 0.3
XMM-LSS	2–10	1712	1.0	9.9 ± 0.4	10.1 ± 0.9	1.98 ± 0.04	3.3 ± 0.3	13.7 ± 0.3

X: Unconstrained or undetermined, ^{a}: Bias factors converted to a common cosmology ($\Omega_\Lambda = 0.7$, $\Omega_m = 0.3$, $\sigma_8 = 0.8$), ^{b}: DMH masses estimated using van den Bosch [54] and Sheth et al. [55], [1]: Ebrero et al. [42], fit ID = 2, assuming no redshift evolution of the correlation length, [2]: Gilli et al. [33], [3]: Basilakos et al. [30], using the LDDE model, [4]: Yang et al. [34], [5]: Miyaji et al. [41], fit ID = 6 with integral constrain, assuming redshift evolution of the correlation length, [6]: Gilli et al. [44], [7]: Allevato et al. [45].

Table 1 summarizes all the discussed results on the clustering of AGN in X-ray surveys with bias factors converted to a common cosmology ($\Omega_\Lambda = 0.7$, $\Omega_m = 0.3$, $\sigma_8 = 0.8$) in the EMSS, Boyle and Mo [19]; RASS, Vikhlinin and Forman [20], Akylas et al. [22]; ROSAT-NEP, Mullis et al. [24]; AXIS, Ebrero et al. [42]; ELAIS-S1, Puccetti et al. [32]; CDFS, Gilli et al. [33]; CDFN, Gilli et al. [33], Yang et al. [34]; XMM-2dF, Basilakos et al. [30]; XMM-LSS, Gandhi et al. [31]; CLASXS, Yang et al. [34]; COSMOS, Gilli et al. [44] Allevato et al. [45]; Swift-BAT, Cappelluti et al. [51]; AEGIS, Coil et al. [48]; AGES, Hickox et al. [47]; ROSAT-SDSS, Krumpe et al. [50], while Figure 3 shows the redshift evolution of the correlation length r_0 as estimated in previous works, according to the legend.

2.1. Techniques of Investigation. The continuously increasing volume and quality of data allowed a parallel improvement of the techniques of investigation. The first surveys of *Einstein*

(see, e.g., [15]) used the autocorrelation function of the unresolved CXB and linked it to the clustering properties of the clustering of X-ray source that produced it.

Modern surveys have mostly estimated correlation function with estimators that use random samples and real data pairs and then estimating physical clustering properties by fitting the correlation function functions with simple power-law models in the form of (2). A detailed description of the method to estimate correlation functions is given in the appendix A. Considering its power, here we give a detailed description of halo modeling which is by far the most reliable formalism to describe clustering of AGN/Galaxies and to determine the environment of a specific DMH tracer.

3. Halo Model

In the hierarchical model of cosmological structure formation, galaxies, group of galaxies, clusters, and so on are built
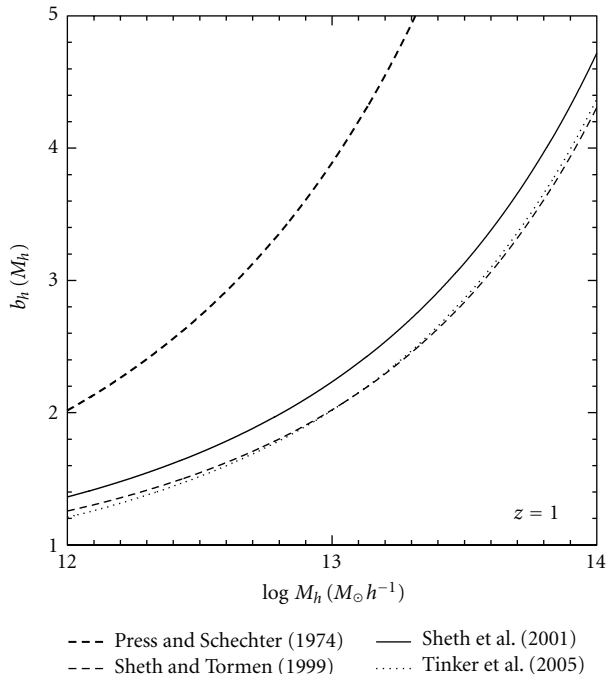
FIGURE 1: Halo bias as function of halo masses for a fixed redshift $z = 1$ and the corresponding predictions of Press and Shechter [56] (long-dashed line), Sheth and Tormen [57] (dashed line), Sheth et al. [55] (solid line), and Tinker et al. [58] (dotted line).

from the same initial perturbation in the underlying dark matter density field. Regions of dark matter denser-than-average collapse to form halos in which structures form. Galaxies and AGN, as well as, groups and clusters are believed to populate the collapsed DMHs.

The theoretical understanding of galaxy clustering has been greatly enhanced through the framework of the *halo model* [58, 64–67]. One can fill DMHs with objects based on a statistical *halo occupation distribution* (HOD), allowing one to model the clustering of galaxies within halos (and thus at nonlinear scales) while providing a self-consistent determination of the bias at linear scales. Similarly the problem of discussing the abundance and spatial distribution of AGN can be reduced to studying how they populate their host halos.

The HOD analysis recasts AGN-clustering measurements into a form that is more physically informative and conducive for testing galaxy/AGN formation theories.

Thus, one can use measurements of AGN two-point correlation functions to constrain the HOD of different sets of AGN and gain information on the nature of DMH in which they live. In fact, the power of the HOD modeling is the capability to transform data on AGN pair counts at small scales into a physical relation between AGN and DMH at the level of individual halos.

The key ingredient needed to describe the clustering properties of AGN is their *halo occupation distribution function* $P_N(M_h)$, which gives the probability of finding N AGN within a single halo as a function of the halo mass, M_h. In the most general case, $P_N(M_h)$ is entirely

specified by all its moments which, in principle, could be observationally determined by studying AGN clustering at any order. Regrettably, AGNs are so rare that their two-point function is already poorly determined, so that it is not possible to accurately measure higher-order statistics. One overcomes this problem by assuming a predefined functional form for the lowest-order moments of $P_N(M_h)$, defining the *halo occupation number* $N(M_h)$ which is the mean value of the halo occupation distribution $N(M_h) = \langle N \rangle (M_h) = \sum_N N P_N(M_h)$. It is convenient to describe $N(M_h)$ in terms of a few parameters whose values will then be constrained by the data.

An accurate description of matter clustering on the basis of the halo approach requires three major ingredients: these halo mass function $n(M_h)$ (the number of DMHs per unit mass and volume), the mass-dependent biasing factor $b(M_h)$, and the density profile of halos. These terms, along with a parametrization of $N(M_h)$, allow us to calculate some useful quantities; the number density of AGN:

$$n_{\text{AGN}} = \int n(M_h) N(M_h) dM_h, \tag{3}$$

the large-scale bias:

$$b = \frac{\int b_h(M_h) N(M_h) n(M_h) dM_h}{\int N(M_h) n(M_h) dM_h}, \tag{4}$$

and the average mass of the host dark halo:

$$M = \frac{\int M_h N(M_h) n(M_h) dM_h}{\int N(M_h) n(M_h) dM_h}. \tag{5}$$

The number density and clustering properties of the DMHs can be easily computed, at any redshift, by means of a set of analytical tools which have been tested and calibrated against numerical simulations [55, 57, 58, 68–72]. Popular choices for both $n(M_h)$ and $b(M_h)$ are the analytical spherical collapse [57] or an ellipsoidal collapse model ([55], see Section 4 for more details). A detailed description of HOD mathematical formalism is given in Appendix B.

3.1. Occupation Number. In the past ten years, a very successful framework for modeling the nonlinear clustering properties of galaxies has been developed and a number of halo models have been presented in the literature. These have been successfully used to describe the abundance and clustering properties of galaxies at both low [58, 65, 73–82] and high [83–87] redshifts, as well as whether these galaxies occupy the centers of the DMH or are satellite galaxies [67, 88].

Partially due to the low number density of AGN, there have been few results in the literature interpreting AGN correlation function using HOD modeling, where the small-scale clustering measurements are essential. Porciani et al. [89] studied the clustering of 2QZ QSO with the halo model to infer the mean number of optically selected quasars which are harboured by a virialized halo of given mass and the characteristic quasar lifetime. Padmanabhan et al. [90] discussed qualitative HOD constraints on their LRG-optical
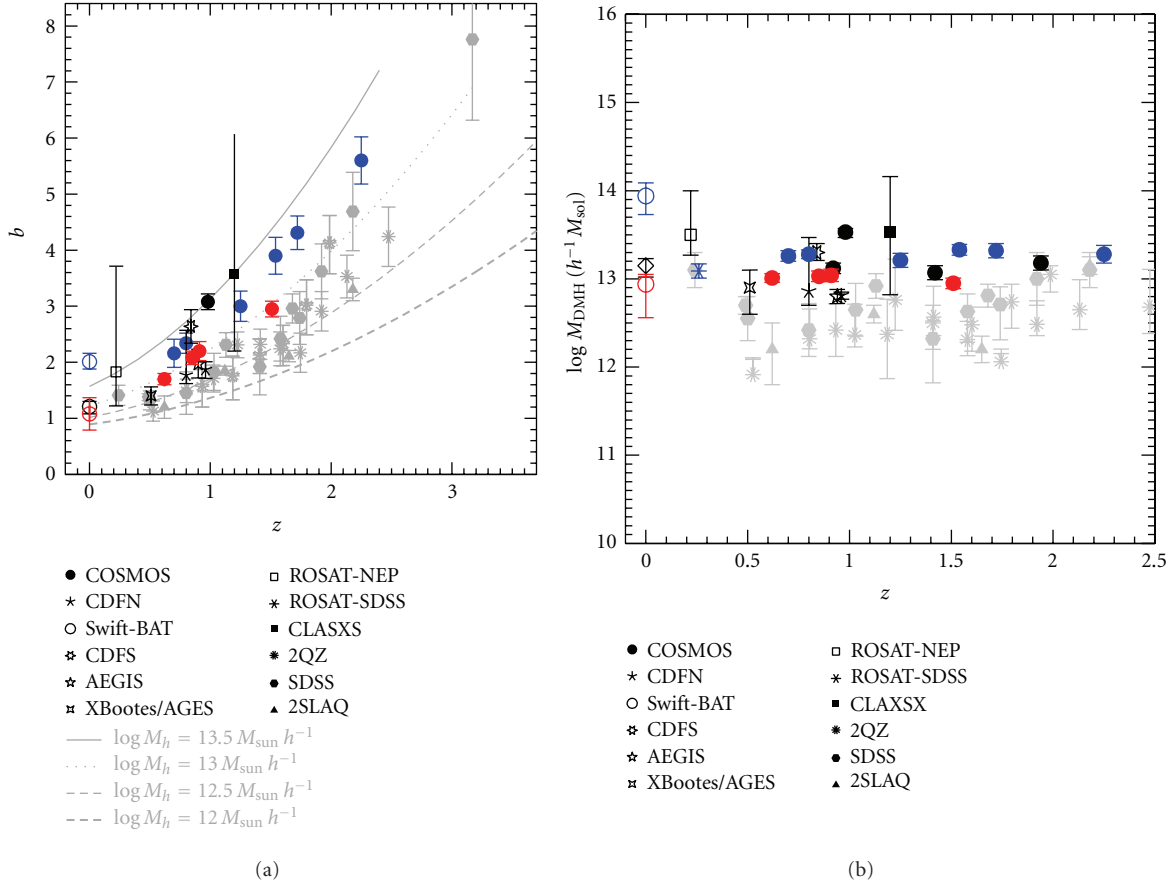
FIGURE 2: Bias factor (a) and mass of AGN hosting halos (b) as a function of redshift for X-ray-selected AGN (black data points), X-ray-selected Type 1 AGN (blue data points), and X-ray selected Type 2 AGN (red data points) as estimated in different surveys (COSMOS, Gilli et al. [44], Allevato et al. [45]; CDFN, Gilli et al. [33], Yang et al. [34]; Swift-BAT, Cappelluti et al. [51]; CDFS, Gilli et al. [33]; AEGIS, Coil et al. [48]; AGES, Hickox et al. [47]; ROSAT-NEP, Mullis et al. [24]; ROSAT-SDSS, Krumpe et al. [50]; CLASXS, Yang et al. [34]). The dashed lines show the expected $b(z)$ of DMHs with different masses according to the legend, based on Sheth et al.[55]. The grey points show results from quasar-quasar correlation measurements using spectroscopic samples from SDSS [59, 60], 2QZ [61, 62], and 2SLAQ [63]. All the previous studies infer the picture that X-ray-selected AGN which are moderate luminosity AGN compared to bright quasars inhabit more massive DMHs than optically selected quasars in the range $z = 0.5$–2.25.

QSO cross-correlation function (CCF), and Shen et al. [91] modelled with the HOD the observed two-point correlation function of 15 binary quasars at $z > 2.9$.

The standard halo approach used for quasars and galaxies is based on the idea that the elements of HOD can be effectively decomposed into two components, separately describing the properties of central and satellite galaxies within the DMH. A simple parametric form used to describe the galaxy HOD is to model the mean occupation number for central galaxies as a step function, that is, $\langle N_{cen} \rangle = 1$ for halos with mass $M \geq M_{min}$ and $\langle N_{cen} \rangle = 0$ for $M < M_{min}$, while the distribution of satellite objects can be well approximated by a Poisson distribution with the mean following a power law, $\langle N_{sat} \rangle = (M/M_1)^{\alpha}$. Previously derived HOD of galaxies show α values ~ 1–1.2 which imply a number of satellite galaxies approximately proportional to M_h.

The clustering properties of X-ray-selected AGN have been modelled with the HOD in two previous works for sources in the *Bootes* field Starikova et al. [92] and in the

ROSAT All-Sky Survey Miyaji et al. [93]. Starikova et al. [92] used the the projections of the two-point correlation function both on the sky plane and in the line of sight to show that *Chandra/Bootes* AGNs are located at the center of DM halos with $M > M_{min} = 4 \times 10^{12} \, \text{h}^{-1} \, M_{\odot}$, assuming a halo occupation described by a step function (zero AGN per halo/subhalo below M_{min} and one above it). They also showed that Chandra/Boötes AGNs are located at the centers of DMHs, limiting the fraction of AGN in noncentral galaxies to be <0.09 at the 95% CL. The central locations of the AGN host galaxies are expected in the merger trigger model because mergers of equally sized galaxies preferentially occur at the centers of DMH [8].

Miyaji et al. [93] modelled the AGN HOD testing the effects of having or not AGN in central galaxies by using the RASS AGN-LRG cross-correlation. In the first scenario, they assumed that all the AGNs are satellites and they visualized the HOD of the LRG as a step function with a step at $\log M_h[h^{-1} M_{\odot} = 13.5]$. While formally they assumed that
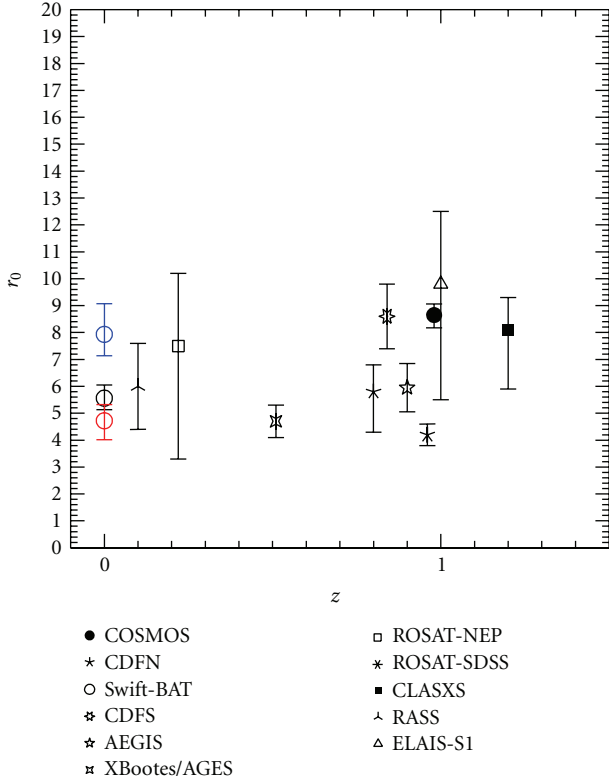
FIGURE 3: Redshift evolution of the correlation length r_0 as estimated in different X-ray surveys (COSMOS, Gilli et al. [44], Allevato et al.[45]; CDFN, Gilli et al. [33], Yang et al. [34]; Swift-BAT, Cappelluti et al. [51]; CDFS, Gilli et al. [33]; AEGIS, Coil et al. [48]; AGES, Hickox et al. [47]; ROSAT-NEP, Mullis et al. [24]; ROSAT-SDSS, Krumpe et al. [50]; CLASXS, Yang et al. [34]; RASS, Akylas et al. [22]; ELAIS-S1, Puccetti et al. [32]).

all AGNs are not in central galaxies, the HOD constraints obtained from this assumption can be applied to satellite and central AGN if the AGN activity in central galaxies of high-mass halos ($\log M_h[h^{-1} M_\odot > 13.5]$) is suppressed. In particular, they used a truncated power-law satellite HOD, with two parameters: the critical DMH mass below which the AGN HOD is zero and the slope α of the HOD for $M_h > M_{cr}$. They also investigated a model where the central HOD is constant and the satellite HOD has a power-law form, both at masses above M_{min}. In all the cases, they rejected $\alpha \sim 1$, finding a marginal preference for an AGN fraction among satellite galaxies which decreases with increasing M_h. They argued that this result might be explained by a decrease of the cross-section for galaxy merging in the environment of richer groups or clusters. In fact, previous observations infer that the AGN fraction is smaller in clusters than in groups [27, 94–96].

It is important to stress that the small number statistics has so far limited the accuracy of correlation function of X-ray AGN at small-scales, especially through the autocorrelation function of the AGN themselves. The situation can be improved by measuring the cross-correlation function of AGN with a galaxy sample that has a much higher space

density, with common sky and redshift coverage as the AGN redshift surveys. The AGN clustering through cross-correlation function with galaxies is emerging in the last years [47, 48, 90, 97–99] and can be used to improve our understanding of how AGNs populate DMH [52, 93].

4. Bias and DMH Mass

In the literature, the bias parameter is often calculated with the power-law fits [24, 34, 41, 48, 50, 100] over scales of 0.1–0.3 $< r_p <$ 10–20 h^{-1} Mpc. The power-law models of the ACF are usually converted to the rms fluctuation over 8 h^{-1} Mpc spheres or are averaged up to the distance of 20 h^{-1} Mpc. While some authors use only large scales ($r_p >$ 1-2 h^{-1} Mpc) to ensure that the linear regime is used, others include smaller scales to have better statistics. As an example, Hickox et al. [47] fitted their data with a biased DMH-projected correlation function.

In the HOD analysis, the bias factor only comes from the 2-halo term ($r_p >$ 1-2 h^{-1} Mpc). Miyaji et al. [93] compared the bias of RASS-AGN from the full HOD model (D.4) with the one estimated using the power-law best fits parameters, finding that the bias estimates are consistent within 1σ. Moreover, using (D.1), one introduces large statistical errors. Allevato et al. [45] found a similar results in comparing the bias of X-ray AGN in COSMOS field from the 2-halo term with (D.3) and the one estimated from the power-law best fits parameters. In Appendix C, we describe the mathematical procedures for the bias parameter calculation commonly used in the literature.

Most of the authors [47, 50, 51] used an analytical expression (as the one described in [55, 57, 58, 69]) to assign a characteristic DMH mass to the hosting halos. The large-scale bias is directly related to the mass function of halos, so that the mass of a halo dictates the halo clustering and the number of such halos. The halo mass can be quantified in terms of the peak height $\nu = \delta_c/\sigma(M_h, z)$, which characterizes the amplitude of density fluctuations from which a halo of mass M_h forms at a given redshift. In generals one assumes $\delta_c = 1.686$ and $\sigma(M_h, z)$ is the linear overdensity variance in spheres enclosing a mean mass M_h. The traditional choice of the mass function and then of the bias has been that of Press and Schechter [56]:

$$b^{PS} = 1 + \frac{\nu^2 - 1}{\delta_c}. \tag{6}$$

A commonly used prescription was derived by Sheth and Tormen [57]:

$$b^{ST} = 1 + \frac{a\nu^2 - 1}{\delta_c} + \frac{2p/\delta_c}{1 + (a\nu^2)^p}, \tag{7}$$

where $a = 0.707$ and $p = 0.3$ or the ellipsoidal collapse formula of Sheth et al. [55]:

$$b^{SMT} = 1 + \frac{1}{\sqrt{a}\delta_c}\left[\sqrt{a}(a\nu^2) + \sqrt{a}b(a\nu^2)^{1-c} \right.$$
$$\left. - \frac{(a\nu^2)^c}{(a\nu^2)^c + b(1-c)\left(\frac{1-c}{2}\right)} \right], \tag{8}$$

where $a = 0.707$, $b = 0.5$, $c = 0.6$ or the recalibrated parameters $a = 0.707$, $b = 0.35$, $c = 0.8$ of Tinker et al. [58]. The ν parameter can be estimated following the appendix of Van den Bosch [54]. Figure 1 shows the bias as function of the halo mass M_h, at $z = 1$, following the predictions of Press and Schechter [56], Sheth and Tormen [57], Sheth et al. [55], and Tinker et al. [58].

Allevato et al. [45] argued that this approach reveals an incongruity due to the fact that the AGN bias used in the formulas above is the average bias of a given AGN sample at a given redshift. In fact, following this approach, one cannot take into account that the average bias is sensitive to the entirety of the mass distribution; different mass distributions with different average masses can give rise to the same average bias.

On the contrary, by using the halo model, the average bias and the average mass of the sample, (D.4), and (5) properly account for the shape of the mass distribution: the average bias depends on the halo number density and on the AGN HOD, integrated over the mass range of the particular AGN sample. They introduced a new method that uses the 2-halo term in estimating the AGN bias factor assuming an AGN HOD described by a δ-function. Following this approach, they properly took into account for the sample variance and the growth of the structures over time associated with the use of large redshift interval of the AGN sample.

On the other hand, Miyaji et al. [93] and Krumpe et al. [52] applied the HOD modeling technique to the RASS AGN-LRG CCF in order to move beyond determining the typical DMH mass based on the clustering signal strength and instead constrain the full distribution of AGN as a function of DMH mass. Along with a parametrization of $N(M_h)$, they estimated the large-scale bias and the typical mass of hosting DM halos using (D.4) and (5). This method improves the clustering analysis because it properly uses the nonlinear growth of matter in the *1-halo* term through the formation and growth of DMHs. These results are significant improvements with respect to the standard method of fitting the signal with a phenomenological power law or using the 2-halo term (see Appendix C).

4.1. X-Ray-Selected AGN Bias, Bias Evolution, and Mass of the Hosting Halos. The majority of the X-ray surveys agree with a picture where X-ray AGNs are typically hosted in DM halos with mass of the order of $12.5 < \log M_{DMH}[h^{-1} M_\odot] < 13.5$, at low ($z < 0.4$) and high ($z \sim 1$) redshift [33, 34, 44, 47, 48, 50–52, 92, 93].

At high redshift, Gilli et al. [33] measured the clustering of X-ray AGN with $z = 0$–4 in both the $\sim 0.1\,\mathrm{deg}^2$ CDFs, finding $b = 1.87^{+0.14}_{-0.16}$ for 240 sources in the northern field and $b = 2.64^{+0.29}_{-0.30}$ for 124 sources in the southern field. At $z \sim 1$, Yang et al. [34] measured the clustering of 233 spectroscopic sources in the 0.4 deg^2 *Chandra* CLASXS area and of 252 spectroscopic sources from the CDFN, both at $z = 0.1$–3. They found $b = 3.58^{+2.49}_{-1.38}$ for the CLASXS AGN and $b = 1.77^{+0.80}_{-0.15}$ for the CDFN field. Gilli et al. [44] studied 538 XMM-COSMOS AGN with $0.1 < z < 3$, and they found a bias factor $b = 3.08^{+0.14}_{-0.14}$ at $\bar{z} \sim 1$. Using

the Millennium simulations, they suggested that XMM-COSMOS AGNs reside in DMH with mass $M_{DMH} > 2.5 \times 10^{12} \, h^{-1} \, M_\odot$. Coil et al. [48] measured the clustering of X-ray AGN at $z = 0.7$–1.4 in the AEGIS field, and they estimated $b = 1.85^{+0.28}_{-0.28}$. Following Zheng et al. [87], they infer from the bias factor that, at $z = 0.94$, the minimum DM halo mass of the X-ray AGN is $>10^{12} \, M_\odot \, h^{-1}$. These results combined with Mountrichas and Georgakakis [49] show that moderate luminosity X-ray-selected AGN live in DMHs with masses $M_h \sim 10^{13} \, h^{-1} \, M_\odot$ at all redshifts since $z \sim 1$. At lower redshift, Hickox et al. [47] analysed 362 AGES X-ray AGN at $\langle z \rangle = 0.51$. The bias factor equal to $b = 1.40 \pm 0.16$ indicates that X-ray AGNs inhabit DM halos of typical mass $\sim 10^{13} \, M_\odot \, h^{-1}$.

In the local Universe, Cappelluti et al. [51] estimated for ~ 200 Swift-BAT AGN a bias equal to $b = 1.21^{+0.07}_{-0.06}$ which corresponds to $\log M_{DM} = 13.15^{+0.09}_{-0.13} \, h^{-1} \, M_\odot$.

Allevato et al. [45] estimated an average mass of the XMM-COSMOS AGN hosting halos equal to $\log M_0[h^{-1} Mpc] = 13.10 \pm 0.06$ at $z \sim 1.2$. They also measured the bias of Type 1 and Type 2 AGN, finding that the latter resides in less massive halos than Type 1 AGN. Only two other works [50, 51] analysed the clustering properties of X-ray-selected Type 1 AGN and Type 2 AGN. Cappelluti et al. [51] estimated the typical DM halo mass hosting type 1 and type 2 Swift-BAT AGN at $z \sim 0$. They measured that these two different samples are characterized by halos with mass equal to $\log M_{DM}[h^{-1} M_\odot] \sim 13.94^{+0.15}_{-0.21}$ and $\sim 12.92^{+0.11}_{-0.38}$, respectively. However, the lack of small separation pair of Type I AGN in the local Universe may have produced systematic deviations which were not accounted in their fits. In Krumpe et al. [50], the bias factor of BL RASS AGN at $z = 0.27$ is consistent with BL AGN residing in halos with mass $\log M_{DM}[h^{-1} M_\odot] = 12.58^{+0.20}_{-0.33}$.

Using the HOD model, Starikova et al. [92] suggested that X-ray Chandra/Bootes AGN is located at the center of DM halos with $M > M_{min} = 4 \times 10^{12} \, h^{-1} \, M_\odot$, while Miyaji et al. [93] estimated for RASS AGN at $z = 0.25, b = 1.32 \pm 0.08$, and a typical mass of the host halos of 13.09 ± 0.08.

The redshift evolution of the clustering of X-ray-selected AGN has been first studied by Yang et al. [34] in the CLAXS+CDFN fields. They measured an increase of the bias factor with redshift, from $b = 0.95 \pm 0.15$ at $z = 0.45$ to $b = 3.03 \pm 0.83$ at $z = 2.07$, corresponding to an average halo mass of $\sim 12.11 \, h^{-1} \, M_\odot$.

Allevato et al. [45] studied the redshift evolution of the bias for a sample of XMM-COSMOS AGN at $z < 2$. They found a bias evolution with time from $b(z = 0.92) = 1.80 \pm 0.19$ to $b(z = 1.94) = 2.63 \pm 0.21$ with a DM halo mass consistent with being constant at $\log M[h^{-1} M_\odot] \sim 13.1$ at all redshifts $z < 2$. They also found evidence of a redshift evolution of the bias factor of XMM-COSMOS Type 1 AGN and Type 2. The bias evolves with redshift at constant average halo mass $\log M_0[h^{-1} M_\odot] \sim 13.3$ for Type 1 AGN and $\log M_0[h^{-1} M_\odot] \sim 13$ for Type 2 AGN at $z < 2.25$ and $z < 1.5$, respectively. In particular, Allevato et al. [45] argued that X-ray selected Type 1 AGNs reside in more massive DMHs compared to X-ray-selected Type 2 AGN at all redshifts at

~2.5σ level, suggesting that the AGN activity is a mass-triggered phenomenon and that different AGN classes are associated with the DM halo mass, irrespective of redshift z.

Krumpe et al. [52] measured the clustering amplitudes of both X-ray RASS and optically selected SDSS broad-line AGNs, as well as for X-ray-selected narrow-line RASS/SDSS AGNs through cross-correlation functions with SDSS galaxies and derive the bias by applying the HOD model directly to the CCFs. They estimated typical DMH masses of broad-line AGNs in the range $\log(M_h/[h^{-1} M_\odot]) = 12.4$–$13.4$, consistent with the halo mass range of typical non-AGN galaxies at low redshifts, and they found no significant difference between the clustering of X-ray-selected narrow-line AGNs and broad-line AGNs up to $z \sim 0.5$.

Figure 2(a) shows the bias parameter and Figure 2(b) the mass of the AGN hosting halos as a function of redshift for X-ray-selected AGN (black data points), X-ray-selected Type 1 AGN (blue data points), and X-ray-selected Type 2 AGN (red data points) as estimated for different surveys (see the legend). The dashed lines show the expected b(z) of typical DM halo masses M_{DMH} based on Sheth et al. [55]. The masses are given in $\log M_{DMH}$ in units of $h^{-1} M_\odot$.

There have been several studies of the bias evolution of optical quasar with the redshift as shown in Figure 2 (grey data points), based on large survey samples such as 2QZ, 2SLAQ, and SDSS [59–63]. These previous studies infer the picture that X-ray-selected AGNs which are moderate luminosity AGN compared to bright quasars inhabit more massive DMHs than optically selected quasars in the range $z = 0.5$–2.25.

Recently, Krumpe et al. [52] verified that the clustering properties between X-ray and optically selected AGN samples are not significantly different in three redshift bins below $z = 0.5$ (the differences are 1.5σ, 0.1σ, and 2.0σ). The reason for the fact that X-ray-selected AGN samples appear to cluster more strongly than optically selected AGNs is still unclear. Allevato et al. [45] and Mountrichas and Georgakakis [49] suggested that the difference in the bias and then in the host DMH masses is due to the different fueling mode of those sources from that of the X-ray-selected moderate luminosity AGN. On the contrary, Krumpe et al. [52] suggested that some of the X-ray clustering studies significantly underestimate their systematic uncertainties and then it may turn out that these measurements are consistent with optical AGN clustering measurements. More high-z AGN clustering measurements based on larger samples are needed to gain a clearer picture.

4.2. AGN Life Time. One of the most important tests for studying the evolution models of AGN is understanding their lifetime. It is widely accepted that AGN is phase of the galaxy life necessary to explain the coevolution of the bulge and the black hole. After a triggering event of which we do not know the nature, yet, the central black hole begins its accretion phase and it is believed that it undergoes several regimes of Eddington rates and bolometric luminosity. Martini and

Weinberg [101] proposed a method to derive the AGN life time by knowing their space density and their DMH host mass.

By knowing the AGN and DMH halo space density at a given luminosity and mass (n_{AGN}, n_{DMH}), one can estimate the duty cycle of the AGN, $\tau_{AGN}(z) = (n_{AGN}(L,z)/n_{DMH}(M,z))(\tau_H(z))$, where $\tau(H(z))$ is the Hubble time at a given redshift. Actually, this method provides only an upper limit since it assumes that the life of halo of a given mass is similar to the Hubble time. A more exhaustive formulation would be $\tau_{AGN}(z) = (n_{AGN}(L,z)/n_{DMH}(M,z))(\tau_{DMH}(z))$, where $\tau_{DMH}(z)$ is the age of a DMH at given redshift. Unfortunately, this quantity cannot be estimated analytically but could be estimated in a statistical way by using hydrodynamic simulations. Several results can be mentioned for these quantities, but their dispersion is very large, therefore we report only some example. At $z = 1$, Gilli et al. [44] obtains that the typical duty cycle of AGN is <1 Gyr. At $z = 0$, Cappelluti et al. [51] have measured a duty cycle in the range 0.2 Gyr–5 Gyr with an expectation value of 0.7 Gyr. Both the measurements are fairly larger than the 40 million years determined by Martini and Weinberg [101] at $z = 2$-3. These differences, however, are not surprising if we assume that the different populations of AGN grow with a different Eddington rate as function of their typical luminosities and/or redshifts [102].

5. Discussion

In this paper, we reviewed the results in the field of X-ray AGN clustering, for energies between 0.1 keV to 55 keV over a period of more than 20 years. The literature has produced an increasingly convincing and consistent picture of the physical quantities derivable from this kind of study. Most of the advancements in the field have been achieved with the improvement of survey capabilities and instruments sensitivity. The availability of simultaneously wide and deep fields, coupled with multiwavelength information, has produced larger and larger samples of spectroscopically confirmed sources. This allowed several teams to refine the techniques needed to estimate the two-point ACF and the quantities derived form it. In particular, we are entering a phase where, at least at $z < 2$, AGN clustering studies will not probably provide any new result unless evaluated with the HOD formalism. Open questions as what is the AGN occupation number and the evolution of HOD define a new barrier which is necessary to break in order to understand the history of X-ray emission from accretion onto AGN. In this respect, samples of X-ray-selected AGN always need a spectroscopical followup to provide a solid base to compute clustering in the real space rather than in the angular space.

Summarizing, the current picture is that X-ray-selected AGNs are highly biased objects with respect to the underlined matter distribution. Such an evidence is clearer when measuring the redshift dependence of AGN bias. At every redshift from $z = 0$ to $z = 2$, AGNs cluster in way similar to DMH of mass of the order of $\log(M_\odot h^{-1}) = 13$. The spread of such a value is of the order 0.3–0.5 dex at 1σ. This

means that the determination of what kind of environment is inhabited by AGN is relatively well constrained and identical at every redshift sampled by X-ray surveys. This allows us to formulate the hypothesis that every phase of AGN activity is mass-triggered phenomenon (i.e., each AGN evolutionary phase is characterized by a critical halo mass).

It is believed that major mergers of galaxies is one of the dominant mechanisms for fueling quasars at high redshift and bright luminosities, while minor interactions, bar instabilities, or tidal disruptions are important at low redshift ($z \lesssim 1$) and low luminosities ($L \lesssim 10^{44} \, \mathrm{erg \, s^{-1}}$) [9, 13, 103, 104]. In the local Universe, for example, the study of the environment of Swift BAT Seyfert galaxies [28] finds a larger fraction of BAT AGNs with disturbed morphologies or in close physical pairs (<30 kpc) compared to matched control galaxies or optically selected AGNs. The high rate of apparent mergers (25%) suggests that AGN activity and merging are critically linked for the moderate luminosity AGN in the BAT sample. Moreover, models of major mergers appear to naturally produce many observed properties of quasars, as the quasar luminosity density, the shape, and the evolution of the quasar luminosity function and the large-scale quasar clustering as a function of L and z (e.g., [8, 46, 105–109]). Quasar clustering at all redshift is consistent with halo masses similar to group scales, where the combination of low velocity dispersion and moderate galaxy space density yields to the highest probability of a close encounter [8, 11]. Moreover, recent detections of an L_X-dependent clustering play in favor of major mergers being the dominant AGN triggering mechanism.

On the other hand, it has became clear that many AGNs are not fueled by major mergers and only a small fraction of AGNs are associated with morphologically disturbed galaxies. Georgakakis et al. [110] and Silverman et al. [96] found that AGNs span a broad range of environments, from the field to massive groups and thus major mergers of galaxies, possibly relevant for the more luminous quasar phenomenon, may not be the primary mechanism for fueling these moderate luminosity AGN.

Georgakakis et al. [111] suggest that bar instabilities and minor interactions are more efficient in producing luminous AGN at $z \lesssim 1$ and not only Seyfert galaxies and low-luminosity AGN as the Hopkins and Henquist [9] model predicts. Cisternas et al. [112] analysed a sample of X-ray-selected AGN host galaxies and a matched control sample of inactive galaxies in the COSMOS field. They found that mergers and interactions involving AGN hosts are not dominant and occur no more frequently than for inactive galaxies. Over 55% of the studied AGN sample that is characterized by $L_{\mathrm{BOL}} \sim 10^{45} \, \mathrm{erg \, s^{-1}}$ and by mass of the host galaxies $M_* \gtrsim 10^{10} \, M_\odot$ are hosted by disk-dominated galaxies, suggesting that secular fuelling mechanisms can be highly efficient.

Moreover, several works on the AGN host galaxies [113–118] show that the morphologies of the AGN host galaxies do not present a preference for merging systems.

At high redshift ($z \sim 2$), recent findings of Schlegel et al. [119] and Rosario et al. [120], who examined a smaller sample of AGN in the ERS-II region of the GOODS-South field, inferred that late-type morphologies are prevalent among the AGN hosts. The role that major galaxy mergers play in triggering AGN activity at $1.5 < z < 2.5$ was also studied in the CDF-S. At $z = 1.5$–3, Schawinski et al. [121] showed that, for X-ray-selected AGN in the Chandra Deep Field South and with typical luminosities of $10^{42} \, \mathrm{erg \, s^{-1}} < L_X < 10^{44} \, \mathrm{erg \, s^{-1}}$, the majority (80%) of the host galaxies of these AGNs have low Srsic indices indicative of disk-dominated light profiles, suggesting that secular processes govern a significant fraction of the cosmic growth of black holes. That is, many black holes in the present-day Universe grew much of their mass in disk-dominated galaxies and not in early-type galaxies or major mergers.

Later, Kocevski et al. [122] found that X-ray-selected AGNs at $z \sim 2$ do not exhibit a significant excess of distorted morphologies while a large fraction reside in late-type galaxies. They also suggested that these late-type galaxies are fueled by the stochastic accretion of cold gas, possibly triggered by a disk instability or minor interaction.

Allevato et al. [45] argued that for moderate luminosity X-ray AGN secular processes such as tidal disruptions or disk instabilities might play a much larger role than major mergers up to $z \sim 2.2$.

It becomes important to study the clustering properties of AGN at high redshift when we assume the peak of the merger-driven accretion. Moreover, given the complexity of AGN triggering, a proper selection of AGN samples, according to the luminosity or the mass of the host galaxies, can help to test a particular model boosting the fraction of AGN host galaxies associated with morphologically disturbed galaxies.

From the evolutionary point of view, the evidence of a bias segregation of optically and X-ray-selected AGN might be a sufficient proof to claim that the two phenomena are sensitive to different environments and therefore likely driven by different triggering mechanisms. A more comprehensive picture will be available when the clustering of different phases of AGN activity will be studied and compared.

Hickox et al. [47] interpreted their clustering results in terms of a general picture for AGN and galaxy evolution which is reproduced in Figure 4. The picture consists of an evolutionary sequence that occurs at different redshifts for halos with different masses. In this scenario, luminous AGN accretion occurs preferentially (through a merger or some secular process) when a host DMH reaches a critical M_{DMH} between 10^{12} and $10^{13} \, M_\odot \, h^{-1}$ (this phase is indicated by the solid ovals). Once a large halo reaches this critical mass, it becomes visible as a ULIRG or SMG (owing to a burst of dusty star formation) or (perhaps subsequently) as a luminous, unobscured quasar. The ULIRG/quasar phase is associated with rapid growth of the SMBH and formation of a stellar spheroid and is followed by the rapid quenching of star formation in the galaxy. Subsequently, the young stellar population in the galaxy ages (producing "green" host galaxy), and the galaxy experiences declining nuclear accretion that may be associated with an X-ray AGN. Eventually, the aging of the young stars leaves a "red" and "dead" early-type galaxy, which experiences intermittent
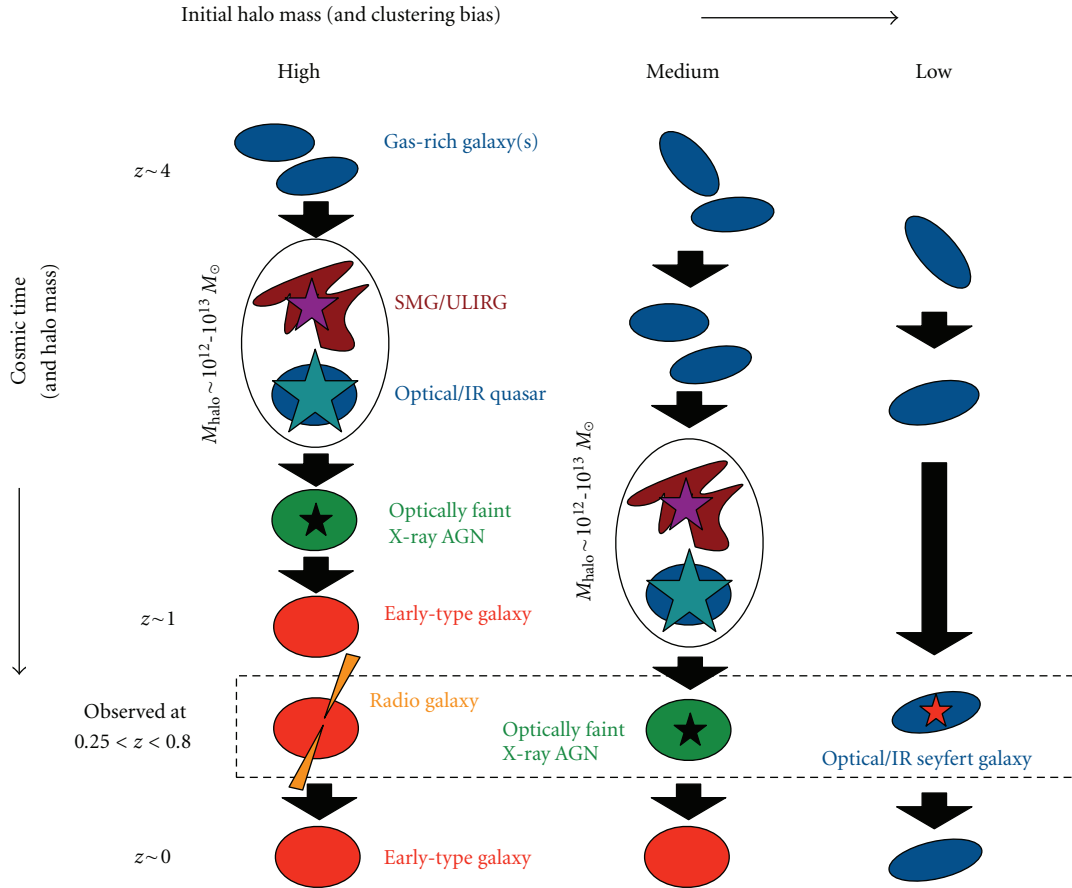
FIGURE 4: Schematic for a simple picture of AGN and host galaxy evolution, taken from Hickox et al. [47] and motivated by the AGN host galaxy and clustering results presented in that study.

"radio-mode" AGN outbursts that heat the surrounding medium. For "medium" initial DMHs, the quasar phase and formation of the spheroid occur later than for the systems with high halo mass, so that, at $z \sim 0.5$, we may observe the green X-ray AGN phase. Even smaller halos never reach the threshold mass for quasar triggering; these still contain star-forming disk galaxies at $z \lesssim 0.8$, and we observe some of them as optical or IR-selected Seyfert galaxies. The dashed box indicates the AGN types (in their characteristic DMH) that would be observable in the redshift range $0.25 < z < 0.8$.

Further steps in the field will require the study of clustering of AGN from $z = 3$ to $z = 6$-7. This will likely lead to the determination of the mass of early DM spheroids who hosted primordial black holes seeds. However, this is a very challenging task since it requires a very deep and wide survey with an almost complete optical followup.

BOSS [123] and BigBOSS [119] will detect high redshift AGNs at $z \sim 2.2$, which will improve AGN clustering measurements at higher redshifts. The only approved mission that at the moment will allow to study the $z = 3$–5 X-ray Universe is eROSITA ([124], launch Dec. 2013) for which an estimate of the completeness of the typical followup is still unavailable. Additionally, the Large Synoptic Survey Telescope ([125], LSST) is expected to identify ~ 2 million AGNs in optical bands. eROSITA and LSST have the potential to significantly improve AGN clustering measurements at low and high redshifts, though only if there are dedicated large spectroscopic follow-up programs. Another strong contribution will come from either Nustar that will likely provide a better view of AGN clustering without the selection biases introduced by photoelectric absorption. Athena, the proposed ESA new generation telescope that will mount a wide field imager on a very large collecting area telescope, will provide a further view on the deep X-ray sky and likely push our knowledge of the high-z X-ray Universe.

In addition to better model the evolution of SMBH environments, a fundamental point to start is to establish the nature of BH seeds at $z = 10$. Such a determination will likely come with the new generation of telescope like JWST and ESO-ELT.

Appendices

A. Deriving the Two-Point Autocorrelation Function

The two-point autocorrelation function ($\xi(r)$, ACF) describes the excess probability over random of finding

a pair with an object in the volume dV_1 and another in the volume dV_2, separated by a distance r so that $dP = n^2[1 + \xi(r)]dV_1 dV_2$, where n is the mean space density. A known effect when measuring pairs separations is that the peculiar velocities combined with the Hubble flow may cause a biased estimate of the distance when using the spectroscopic redshift. To avoid this effect, it is usually computed the projected ACF [126]: $w(r_p) = 2\int_0^{\pi_{max}} \xi(r_p, \pi)d\pi$, where r_p is the distance component perpendicular to the line of sight and π parallel to the line of sight [127]. It can be demonstrated that, if the ACF is expressed as $\xi(r) = (r/r_0)^{-\gamma}$, then

$$w(r_p) = A(\gamma) r_0^\gamma r_p^{1-\gamma}, \qquad \text{(A.1)}$$

where $A(\gamma) = \Gamma(1/2)\Gamma[(\gamma - 1)/2]/\Gamma(\gamma/2)$ [21].

The ACF is mostly estimated by using the minimum variance estimator described by Landy and Szalay [128]:

$$\xi(r_p, \pi) = \frac{DD - 2DR + RR}{RR}, \qquad \text{(A.2)}$$

where DD, DR, and RR are the normalized number of data-data, data-random, and random-random source pairs, respectively. Equation (A.2) indicates that an accurate estimate of the distribution function of the random samples is crucial in order to obtain a reliable estimate of $\xi(r_p, \pi)$. Note that other estimators have been proposed in the literature, but the Landy and Szalay [128] one has been shown to provide the smallest statistical variance. Such a formalism can be easily adopted when computing the angular or the redshift space correlation function, with the only difference that the evaluation is made on a single dimension. Several observational biases must be taken into account when generating a random sample of objects in a X-ray-flux limited survey. In particular, in order to reproduce the selection function of the survey, one has to carefully reproduce the space and flux distributions of the sources, since the sensitivity in X-ray surveys is not homogeneous on the detector and therefore on the sky. This points out the necessity of creating a random sample which includes as many selection effects as possible since the estimate of $\xi(r)$ (or $w(\theta)$) is strongly dependent on RR (see (A.2)). Moreover, in several cases, optical followup of the X-ray source is not 100% complete, therefore one must carefully reproduce the mask effect. What is usually done is that to create random samples in 3D, sources are placed at the same angular position of the real sources and redshift are randomly drawn from a smoothed redshift distribution of the real sources. If instead the spectral completeness is close to 100%, then the right procedures are to occupy the survey volume with random sources drawn from a L-z dependent luminosity function and accept check if they would be observable using a sensitivity map. An important choice for obtaining a reliable estimate of $w(r_p)$ is to set π_{max} in the calculation of the integral above. One should avoid values of π_{max} too large since they would add noise to the estimate of $w(r_p)$. If, instead, π_{max} is too small one could not recover all the signal. Uncertainties in the ACF are usually evaluated with a bootstrap resampling technique, but it is worth noting

that, in the literature, several methods are adopted for errors estimates in two-point statistics, (See [129] for a detailed description). It is known that Poisson estimators generally underestimate the variance because they do consider that points in ACF are not statistically independent. Jackknife resampling method, where one divides the survey area in many sub fields and iteratively recomputes correlation functions by excluding one subfield at a time, generally gives a good estimate of errors. But it requires that sufficient number of almost statistically independent subfields, this is not the case for most of X-ray surveys where the source statistics is moderately low. Coil et al. [48] estimated the error bars on the two-point correlation function including both Poisson and cosmic variance errors estimated, using DEEP2 mock catalogs derived from the Millenium Run simulations.

B. Limber's Deprojection

The 2D angular correlation function (ACF) is a projection of the real-space 3D ACF of the sources along the line of sight. In the following discussions and thereafter, r is in comoving coordinates. The relation between the 2D (angular) ACF and the 3D ACF is expressed by the Limber equation (e.g., [21]). Under the assumption that the scale length of the clustering is much smaller than the distance to the object, this reduces to

$$w(\theta)N^2 = \int \left(\frac{dN}{dZ}\right)^2 \\ \int \xi\left(\sqrt{[d_A(z)\theta^2] + l^2(1+z)}\right)\left(\frac{dl}{dz}\right)^{-1} dl\, dz, \qquad \text{(B.1)}$$

where $d_A(z)$ is the angular distance, N is the total number of sources, and dN/dz is the redshift distribution (per z) of the sources. The redshift evolution of the 3D correlation function is customarily expressed by

$$\xi(r, z) = \left(\frac{r}{r_0}\right)^{-\gamma}(1+z)^{-3-\epsilon+\gamma}, \qquad \text{(B.2)}$$

where $\epsilon = -3$ and $\epsilon = \gamma - 3$ correspond to the case where the correlation length is constant in physical and comoving coordinates, respectively. In these notations, the zero-redshift 3D correlation length r_0 can be related to the angular correlation length θ_0 by

$$r_0^\gamma = \left(\frac{N^2}{S}\right)\theta_0^{\gamma-1},$$

$$S = H_\gamma \int \left(\frac{dN}{dZ}\right)^2 \left[\frac{cd\tau(z)}{dz}\right]^{-1} \\ d_A^{1-\gamma}(1+z)^{-3-\epsilon}dz, \qquad \text{(B.3)}$$

$$H_\gamma = \frac{\Gamma[(\gamma - 1)/2]\Gamma(1/2)}{\Gamma(1/2)},$$

where $\tau(z)$ is the look-back time. We also define the comoving correlation length

$$r_0(z_{eff}^-) = r_0(1 + z_{eff}^-)^{-3-\epsilon+\gamma}, \qquad \text{(B.4)}$$

at the effective redshift z_{eff}^-, which is the median redshift of the contribution to the angular correlation (the integrand of the second term). An essential ingredient of the deprojection process is the redshift distribution of the sources, and, when individual redshifts are not available, this is derived from integration of the luminosity function.

C. 1-Halo and 2-Halo Terms in the HOD Formalism

In the halo model approach, the two-point correlation function of AGN is the sum of two contributions: the first term (*1-halo term*) is due to the correlation between objects in the same halo and the second term (*2-halo term*) arises because of the correlation between two distinct halos:

$$\xi(r) = \xi_{1h}(r) + \xi_{2h}(r). \tag{C.1}$$

Recent articles prefer to express $w = (1 + \xi_{1h}) + \xi_{2h}$ [58, 67, 130], instead of $\xi = \xi_{1h} + \xi_{2h}$, as used in older articles. This is because $1+\xi$ represents a quantity that is proportional to the number of pairs $\propto [1 + \xi_{1h}] + [1 + \xi_{2h}]$. In this new convention, the projected correlation function ξ_{1h} represents the projection of $1 + \xi_{1h}$ rather than ξ_{1h}.

Similarly, one expresses the power spectrum of the distribution of the AGN in terms of the 1- and 2-halo term contributions:

$$P(k) = P_{1h}(k) + P_{2h}(k), \tag{C.2}$$

and then the projected correlation function as

$$\begin{aligned} w_{p,1h}(r_p) &= \int \frac{k}{2\pi} P_{1h}(k) J_0(kr_p) dk, \\ w_{p,2h}(r_p) &= \int \frac{k}{2\pi} P_{2h}(k) J_0(kr_p) dk, \end{aligned} \tag{C.3}$$

where $J_0(x)$ is the zeroth-order Bessel function of the first kind.

Several parametrizations exist in literature for representing the DMH profile [66, 131, 132], and the Navarro et al. [6] (NFW) profile is a popular choice. If $y(k, M_h)$ expresses the Fourier transform of the NFW profile of the DMH with mass M_h, normalized such that volume integral up to the virial radius is unity, then the one-halo term of the power spectrum can be written as

$$P_{1h}(k) = \frac{1}{n_{AGN}^2} \int n(M_h) N(M_h) |y(k, M_h)|^2 dM_h. \tag{C.4}$$

Assuming the linear halo bias model [68], the two-halo term of the power spectrum reduces to

$$P_{2h}(k) = P_m(k) \left[\frac{1}{n_{AGN}} \int n(M_h) b(M_h) y(k, M_h) dM_h \right]^2. \tag{C.5}$$

Since the clustering on large scales is dominated by the two-halo term, it is fairly insensitive to the assumption of AGN

distribution inside the hosting halo [75]. It should be noted that since $y \sim 1$ on large scales (e.g., scales much larger than the virial radius of halos), on such scales the two-halo term can be rewritten as

$$P_{2h}(k) \approx b^2 P_m(k, z), \tag{C.6}$$

or, in terms of projected correlation function,

$$w_{p,2h}(r_p) = b^2 w_{m,2h}(r_p), \tag{C.7}$$

where b is the bias parameter of the sample and $w_{m,2h}$ is the DM-projected correlation function. For the matter power spectrum, $P_m(k)$, one can use the primordial power spectrum with a fixed n_s and a transfer function calculated using the fitting formula of Eisenstein and Hu [133] or the nonlinear form given by Smith et al. [134] and Tinker et al. [58].

D. Bias Parameter Calculation

In the majority of works on clustering of X-ray AGN [24, 33, 34, 48, 50, 51], the standard approaches used to estimate the bias are based on the power-law fit parameters of the AGN correlation function. This method assumes that the projected correlation function is well fitted by a power-law and the bias factors are derived from the best fit parameters r_0 and γ of the clustering signal at large scale. Using the power-law fit, one can estimate the AGN bias factor using the power-law best fit parameters:

$$b_{PL} = \frac{\sigma_{8,AGN}(z)}{\sigma_{DM}(z)}, \tag{D.1}$$

where $\sigma_{8,AGN}(z)$ is the rms fluctuations of the density distribution over the sphere with a comoving radius of $8\,Mpc\,h^{-1}$, $\sigma_{DM}(z)$ is the dark matter correlation function evaluated at $8\,Mpc\,h^{-1}$, normalized to a value of $\sigma_{DM}(z = 0) = 0.8$. For a power-law correlation function, this value can be calculated by [21]:

$$(\sigma_{8,AGN})^2 = J_2(\gamma) \left(\frac{r_0}{8\,Mpc\,h^{-1}} \right)^\gamma, \tag{D.2}$$

where $J_2(\gamma) = 72/[(3 - \gamma)(4 - \gamma)(6 - \gamma)2^\gamma]$.

Differently in the halo model approach, the 2-halo term of the projected correlation function, which dominates at large scales, can be considered in the regime of linear density fluctuations. In the linear regime, AGNs are biased tracers of the dark matter distribution and the bias factor is described by:

$$b = \left(\frac{w_{p,1h}(r_p)}{w_{m,2h}(r_p)} \right)^{1/2}. \tag{D.3}$$

HOD modeling is currently the optimal method to establish the large-scale bias parameter, provided the parametrization of $N(M_h)$, by using

$$b = \frac{\int b_h(M_h) N(M_h) n(M_h) dM_h}{\int N(M_h) n(M_h) dM_h} \tag{D.4}$$

assuming the halo mass function $n(M_h)$ and the halo bias factor $b(M_h)$.

In fact, power-law fit bias measurements commonly use smaller scales ($<$1-2 h^{-1} Mpc) that are in the 1-halo term in order to increase the statistical significance. If power-law fits are restricted only to larger scales, the method suffers from the problem that the lowest scale, where the linear biasing scheme can still be applied, varies from sample to sample and remains ambiguous.

HOD modeling allows, in principle, the use of the full range of scales since the method first determines the 1- and 2-halo terms and then constrains the linear using data down to the smallest r_p values that are dominated by the 2-halo term for each individual sample.

Krumpe et al. [52] estimated the RASS-AGN bias following the power-law (D.1) and the HOD (D.4) approach, pointing out that, using the first method, the errors on the bias are much larger, but the values are statistically consistent which those derived from the HOD model fits. Allevato et al. [45] found similar results in estimating the COSMOS-AGN bias following (D.1) and (D.3).

In order to derive a reliable picture of AGN clustering, bias parameters should be inferred from HOD modeling, or at least from the comparison of the correlation function with that of the DM only in the linear regime, because systematic errors based on power-law bias parameters will be larger than the statistical uncertainties of the clustering measurement.

Acknowledgments

References

[1] R. Giacconi, J. Bechtold, G. Branduardi et al., "A high-sensitivity X-ray survey using the Einstein Observatory and the discrete source contribution to the extragalactic X-ray background," *Astrophysical Journal*, vol. 234, pp. L1–L17, 1979.

[2] J. Magorrian, S. Tremaine, D. Richstone et al., "The demography of massive dark objects in galaxy centers," *Astronomical Journal*, vol. 115, no. 6, pp. 2285–2305, 1998.

[3] N. I. Shakura and R. A. Sunyaev, "A theory of the instability of disk accretion on to black holes and the variability of binary X-ray sources, galactic nuclei and quasars," *Monthly Notices of the Royal Astronomical Society*, vol. 175, pp. 613–32, 1976.

[4] R. Bergamini, P. Londrillo, and G. Setti, "The cosmic black-body radiation and the inverse compton effect in the radio galaxies: the X-ray background," *Il Nuovo Cimento B Series*, vol. 52, no. 2, pp. 495–506, 1967.

[5] G. Hasinger, R. Burg, R. Giacconi et al., "A deep X-ray survey in the lockman-hole and the soft X-ray N-log," *Astronomy and Astrophysics*, vol. 275, no. 1, p. 1, 1993.

[6] J. F. Navarro, C. S. Frenk, and S. D. M. White, "A universal density profile from hierarchical clustering," *Astrophysical Journal*, vol. 490, no. 2, pp. 493–508, 1997.

[7] P. F. Hopkins, A. Lidz, L. Hernquist et al., "The co-formation of spheroids and quasars traced in their clustering," *Astrophysical Journal*, vol. 662, no. 1, pp. 110–130, 2007.

[8] P. F. Hopkins, L. Hernquist, T. J. Cox, and D. Kerbs, "A cosmological framework for the co-evolution of quasars, supermassive black holes, and elliptical galaxies. i. galaxy mergers and quasar activity," *Astrophysical Journal, Supplement Series*, vol. 175, no. 2, pp. 356–389, 2008.

[9] P. F. Hopkins and L. Hernquist, "A characteristic division between the fueling of quasars and seyferts: five simple tests," *Astrophysical Journal*, vol. 694, no. 1, pp. 599–609, 2009.

[10] J. D. Silverman, P. Kampczyk, K. Jahnke et al., "The impact of galaxy interactions on active galactic nucleus activity in zCOSMOS," *The Astrophysical Journal*, vol. 743, no. 1, article 2, 2011.

[11] D. H. McIntosh, Y. Guo, H. J. Mo, F. van den Bosch, and X. Yan, "The SDSS view of galaxy mergers and their environments," *Bulletin of the American Astronomical Society*, vol. 41, p. 244, 2009.

[12] M. Milosavljević, D. Merritt, and L. C. Ho, "Contribution of stellar tidal disruptions to the X-ray luminosity function of active galaxies," *Astrophysical Journal*, vol. 652, no. 1, pp. 120–125, 2006.

[13] P. F. Hopkins, L. Hernquist, T. J. Cox, T. Di Matteo, B. Robertson, and V. Springel, "A unified, merger-driven model of the origin of starbursts, quasars, the cosmic X-ray background, supermassive black holes, and galaxy spheroids," *Astrophysical Journal, Supplement Series*, vol. 163, no. 1, pp. 1–49, 2006.

[14] D. Larson, J. Dunkley, G. Hinshaw et al., "Seven-year wilkinson microwave anisotropy probe (WMAP) observations: power spectra and WMAP-derived parameters," *Astrophysical Journal, Supplement Series*, vol. 192, article 16, 2011.

[15] X. Barcons and A. C. Fabian, "Fluctuations in the X-ray background and the large-scale structure of the universe," *Monthly Notices of the Royal Astronomical Society*, vol. 230, pp. 189–206, 1988.

[16] F. J. Carrera and X. Barcons, "The spatial distribution of cosmic X-ray sources from the isotropy of the soft X-ray background," *Monthly Notices of the Royal Astronomical Society*, vol. 257, no. 3, pp. 507–512, 1992.

[17] I. Georgantopoulos, G. C. Stewart, T. Shanks, R. E. Griffiths, and B. J. Boyle, "A deep ROSAT survey. II—observations of the isotropy of the 1-2 keV X-ray background," *Monthly Notices of the Royal Astronomical Society*, vol. 262, no. 3, pp. 619–626, 1993.

[18] A. Soltan and G. Hasinger, "The angular correlation function of the soft X-ray background," *Astronomy and Astrophysics*, vol. 288, no. 1, pp. 77–88, 1994.

[19] B. J. Boyle and H. J. Mo, "The clustering of QSOs at low redshift," *Monthly Notices of the Royal Astronomical Society*, vol. 260, no. 4, pp. 925–928, 1993.

[20] A. Vikhlinin and W. Forman, "Detection of the angular correlation of faint X-ray sources," *Astrophysical Journal*, vol. 455, no. 2, pp. L109–L113, 1995.

[21] P. J. E. Peebles, *The Large Scale Structure of the Universe*, Princeton University Press, Princeton, NJ, USA, 1980.

[22] A. Akylas, I. Georgantopoulos, and M. Plionis, "The angular correlation function of the ROSAT all-sky survey bright source catalogue," *Monthly Notices of the Royal Astronomical*

Society, vol. 318, no. 4, pp. 1036–1040, 2000.

[23] X. Barcons, F. J. Carrera, M. T. Ceballos, and S. Mateos, "X-ray sources as tracers of the large-scale structure in the universe ," in *Proceedings of the X-Ray Astronomy: Stellar Endpoints,AGN, and the Diffuse X-ray Background*, vol. 599, pp. 3–12, 2001.

[24] C. R. Mullis, J. P. Henry, I. M. Gioia et al., "Spatial correlation function of X-ray-selected active galactic nuclei," *Astrophysical Journal*, vol. 617, no. 1, pp. 192–208, 2004.

[25] M. Cappi, P. Mazzotta, M. Elvis et al., "Chandra study of an overdensity of x-ray sources around two distant (z ∼ 0.5) clusters," *Astrophysical Journal*, vol. 548, no. 2, pp. 624–638, 2001.

[26] N. Cappelluti, M. Cappi, M. Dadina et al., "X-ray source overdensities in *Chandra* distant cluster fields: a new probe to map the cosmic tapestry?" *Astronomy and Astrophysics*, vol. 430, no. 1, pp. 39–45, 2005.

[27] E. Koulouridis and M. Plionis, "Luminous X-ray active galactic nuclei in clusters of galaxies," *Astrophysical Journal*, vol. 714, no. 2, pp. L181–L184, 2010.

[28] M. Koss, R. Mushotzky, S. Veilleux, and L. Winter, "Merging and clustering of the swift bat AGN sample," *Astrophysical Journal*, vol. 716, no. 2, pp. L125–L130, 2010.

[29] S. Basilakos, M. Plionis, A. Georgakakis et al., "The XMM-Newton/2dF survey—III. Comparison between optical and X-ray cluster detection methods," *Monthly Notices of the Royal Astronomical Society*, vol. 351, no. 3, pp. 989–996, 2004.

[30] S. Basilakos, M. Plionis, A. Georgakakis, and I. Georgantopoulos, "The XMM-Newton/2dF survey—VI. Clustering and bias of the soft X-ray point sources," *Monthly Notices of the Royal Astronomical Society*, vol. 356, no. 1, pp. 183–191, 2005.

[31] P. Gandhi, O. Garcet, L. Disseau et al., "The XMM large scale structure survey: properties and two-point angular correlations of point-like sources," *Astronomy and Astrophysics*, vol. 457, no. 2, pp. 393–404, 2006.

[32] S. Puccetti, F. Flore, V. D'Elia et al., "The XMM-Newton survey of the ELAIS-S1 field I. Number counts, angular correlation function and X-ray spectral properties," *Astronomy and Astrophysics*, vol. 457, no. 2, pp. 501–515, 2006.

[33] R. Gilli, E. Daddi, G. Zamorani et al., "The spatial clustering of X-ray selected AGN and galaxies in the Chandra Deep Field South and North," *Astronomy and Astrophysics*, vol. 430, no. 3, pp. 811–825, 2005.

[34] Y. Yang, R. F. Mushotzky, A. J. Barger, and L. L. Cowie, "Spatial correlation function of the Chandra-selected active galactic nuclei," *Astrophysical Journal*, vol. 645, no. 1, pp. 68–82, 2006.

[35] G. Hasinger, N. Cappelluti, H. Brunner et al., "The XMM-Newton wide-field survey in the COSMOS field. I. Survey description," *Astrophysical Journal, Supplement Series*, vol. 172, no. 1, pp. 29–37, 2007.

[36] N. Cappelluti, G. Hasinger, M. Brusa et al., "The XMM-Newton wide-field survey in the COSMOS field. II. X-ray data and the log N-log S relations," *Astrophysical Journal, Supplement Series*, vol. 172, no. 1, pp. 341–352, 2007.

[37] N. Cappelluti, M. Brusa, G. Hasinger et al., "The XMM-Newton wide-field survey in the COSMOS field," *Astronomy and Astrophysics*, vol. 497, no. 2, pp. 635–648, 2009.

[38] M. Elvis and Chandra-COSMOS Team, "The chandra-COSMOS survey: first results," *Bullettin of the American Astronomical Society*, vol. 39, no. 4, p. 899, 2007.

[39] S. Puccetti, C. Vignali, and N. Cappelluti, "The chandra survey of the cosmos field. II. source detection and photometry," *The Astrophysical Journal Supplement Series*, vol. 185, no. 2, article 586, 2009.

[40] S. J. Lilly, O. Le Fèvre, A. Renzini et al., "zCOSMOS: a large VLT/VIMOS redshift survey covering 0 < z < 3 in the COSMOS field 1," *Astrophysical Journal, Supplement Series*, vol. 172, no. 1, pp. 70–85, 2007.

[41] T. Miyaji, G. Zamorani, N. Cappelluti et al., "The XMM-Newton wide-field survey in the COSMOS field. V angular clustering of the X-ray point sources," *Astrophysical Journal, Supplement Series*, vol. 172, no. 1, pp. 396–405, 2007.

[42] J. Ebrero, S. Mateos, G. C. Stewart, F. J. Carrera, and M. G. Watson, "High-precision multi-band measurements of the angular clustering of X-ray sources," *Astronomy and Astrophysics*, vol. 500, no. 2, pp. 749–762, 2009.

[43] A. Elyiv, N. Clerc, M. Plionis et al., "Angular correlation functions of X-ray point-like sources in the full exposure XMM-LSS field," *Astronomy and Astrophysics*, vol. 537, article A131, 2012.

[44] R. Gilli, G. Zamorani, T. Miyaji et al., "The spatial clustering of X-ray selected AGN in the XMM-COSMOS field," *Astronomy and Astrophysics*, vol. 494, no. 1, pp. 33–48, 2009.

[45] V. Allevato, A. Finoguenov, N. Cappelluti et al., "The XMM-newton wide field survey in the cosmos field: redshift evolution of agn bias and subdominant role of mergers in triggering moderate-luminosity AGNs at redshifts up to 2.2," *Astrophysical Journal*, vol. 736, no. 2, article 99, 2011.

[46] S. Bonoli, F. Marulli, V. Springel, S. D. M. White, E. Branchini, and L. Moscardini, "Modelling the cosmological co-evolution of supermassive black holes and galaxies—II. the clustering of quasars and their dark environment," *Monthly Notices of the Royal Astronomical Society*, vol. 396, no. 1, pp. 423–438, 2009.

[47] R. C. Hickox, C. Jones, W. R. Forman et al., "Host galaxies, clustering, Eddington ratios, and evolution of radio, X-ray, and infrared-selected AGNs," *Astrophysical Journal Letters*, vol. 696, no. 1, pp. 891–919, 2009.

[48] A. L. Coil, A. Georgakakis, J. A. Newman et al., "Aegis: the clustering of x-ray active galactic nucleus relative to galaxies at z ∼ 1," *Astrophysical Journal Letters*, vol. 701, no. 2, pp. 1484–1499, 2009.

[49] G. Mountrichas and A. Georgakakis, "The clustering of X-ray-selected active galactic nuclei at $z = 0.1$," *Monthly Notices of the Royal Astronomical Society*, vol. 420, no. 1, pp. 514–525, 2012.

[50] M. Krumpe, T. Miyaji, and A. L. Coil, "The spatial clustering of rosat all-sky survey AGNs. I. the cross-correlation function with sdss luminous red galaxies," *Astrophysical Journal*, vol. 713, no. 1, pp. 558–572, 2010.

[51] N. Cappelluti, M. Burlon D. Aiello et al., "Active galactic nuclei clustering in the local universe: an unbiased picture from swift-BAT," *The Astrophysical Journal Letters*, vol. 716, no. 2, pp. L209–L213, 2010.

[52] M. Krumpe, T. Miyaji, A. L. Coil, and H. Aceves, "The spatial clustering of ROSAT All-Sky Survey active galactic nuclei. III. Expanded sample and comparison with optical active galactic nuclei," *Astrophysical Journal*, vol. 746, article 1, 2012.

[53] M. Plionis, M. Rovilos, S. Basilakos, I. Georgantopoulos, and F. Bauer, "Luminosity-dependent X-ray active galactic nucleus clustering?" *The Astrophysical Journal*, vol. 674, no. 1, pp. L5–L8, 2008.

[54] F. C. van den Bosch, "The universal mass accretion history

of cold dark matter haloes," *Monthly Notices of the Royal Astronomical Society*, vol. 331, no. 1, pp. 98–110, 2002.

[55] R. K. Sheth, H. J. Mo, and G. Tormen, "Ellipsoidal collapse and an improved model for the number and spatial distribution of dark matter haloes," *Monthly Notices of the Royal Astronomical Society*, vol. 323, no. 1, pp. 1–12, 2001.

[56] W. H. Press and P. Schechter, "Formation of galaxies and clusters of galaxies by self-similar gravitational condensation," *Astrophysical Journal*, vol. 187, pp. 425–438, 1974.

[57] R. K. Sheth and G. Tormen, "Large-scale bias and the peak background split," *Monthly Notices of the Royal Astronomical Society*, vol. 308, no. 1, pp. 119–126, 1999.

[58] J. L. Tinker, D. H. Weinberg, Z. Zheng, and I. Zehavi, "On the mass-to-light ratio of large-scale structure," *Astrophysical Journal*, vol. 631, no. 1, pp. 41–58, 2005.

[59] N. P. Ross, Y. Shen, M. A. Strauss et al., "Clustering of low-redshift (z ≤ 2.2) quasars from the sloan digital sky survey," *Astrophysical Journal*, vol. 697, no. 2, pp. 1634–1655, 2009.

[60] Y. Shen, M. A. Strauss, N. P. Ross et al., "Quasar clustering from SDSS DR5: dependences on physical properties," *Astrophysical Journal Letters*, vol. 697, no. 2, pp. 1656–1673, 2009.

[61] S. M. Croom, B. J. Boyle, T. Shanks et al., "The 2dF QSO redshift survey - XIV. Structure and evolution from the two-point correlation function," *Monthly Notices of the Royal Astronomical Society*, vol. 356, no. 2, pp. 415–438, 2005.

[62] C. Porciani and P. Norberg, "Luminosity- and redshift-dependent quasar clustering," *Monthly Notices of the Royal Astronomical Society*, vol. 371, no. 4, pp. 1824–1834, 2006.

[63] J. Da Ângela, T. Shanks, S. M. Croom et al., "The 2dF-SDSS LRG and QSO survey: QSO clustering and the L-z degeneracy," *Monthly Notices of the Royal Astronomical Society*, vol. 383, no. 2, pp. 565–580, 2008.

[64] G. Kauffmann, A. Nusser, and M. Steinmetz, "Galaxy formation and large-scale bias," *Monthly Notices of the Royal Astronomical Society*, vol. 286, no. 4, pp. 795–811, 1997.

[65] J. A. Peacock and R. E. Smith, "Halo occupation numbers and galaxy bias," *Monthly Notices of the Royal Astronomical Society*, vol. 318, no. 4, pp. 1144–1156, 2000.

[66] A. Cooray and R. Sheth, "Halo models of large scale structure," *Physics Report*, vol. 372, no. 1, pp. 1–129, 2002.

[67] Z. Zheng, A. A. Berlind, D. H. Weinberg et al., "Theoretical models of the halo occupation distribution: separating central and satellite galaxies," *Astrophysical Journal*, vol. 633, no. 2, pp. 791–809, 2005.

[68] H. J. Mo and S. D. M. White, "An analytic model for the spatial clustering of dark matter haloes," *Monthly Notices of the Royal Astronomical Society*, vol. 282, no. 2, pp. 347–361, 1996.

[69] S. Basilakos, M. Plionis, and C. Ragone-Figueroa, "The halo mass-bias redshift evolution in the ACDM cosmology," *Astrophysical Journal*, vol. 678, no. 2, pp. 627–634, 2008.

[70] J. L. Tinker, B. E. Robertson, A. V. Kravtsov et al., "The large-scale bias of dark matter halos: numerical calibration and model tests," *Astrophysical Journal*, vol. 724, no. 2, pp. 878–886, 2010.

[71] A. Pillepich, C. Porciani, and O. Hahn, "Halo mass function and scale-dependent bias from N-body simulations with non-Gaussian initial conditions," *Monthly Notices of the Royal Astronomical Society*, vol. 402, no. 1, pp. 191–206, 2010.

[72] C.-P. Ma, M. Maggiore, A. Riotto, and J. Zhang, "The bias and mass function of dark matter haloes in non-Markovian

extension of the excursion set theory," *Monthly Notices of the Royal Astronomical Society*, vol. 411, no. 4, pp. 2644–2652, 2011.

[73] Seljak, "Analytic model for galaxy and dark matter clustering," *Monthly Notices of the RoyalAstronomical Society*, vol. 318, p. 2035, 2000.

[74] R. Scoccimarro, R. K. Sheth, L. Hui, and B. Jain, "How many galaxies fit in a halo? Constraints on galaxy formation efficiency from spatial clustering," *Astrophysical Journal*, vol. 546, no. 1, pp. 20–34, 2001.

[75] A. A. Berlind and D. H. Weinberg, "The halo occupation distribution: toward an empirical determination of the relation between galaxies and mass," *Astrophysical Journal*, vol. 575, no. 2, pp. 587–616, 2002.

[76] C. Marinoni and M. J. Hudson, "The mass-to-light function of virialized systems and the relationship between their optical and X-ray properties," *Astrophysical Journal*, vol. 569, no. 1, pp. 101–111, 2002.

[77] M. Magliocchetti and C. Porciani, "The halo distribution of 2dF galaxies," *Monthly Notices of the Royal Astronomical Society*, vol. 346, no. 1, pp. 186–198, 2003.

[78] F. C. van den Bosch, X. Yang, and H. J. Mo, "Linking early- and late-type galaxies to their dark matter haloes," *Monthly Notices of the Royal Astronomical Society*, vol. 340, no. 3, pp. 771–792, 2003.

[79] X. Yang, H. J. Mo, and F. C. Van den Bosch, "Constraining galaxy formation and cosmology with the conditional luminosity function of galaxies," *Monthly Notices of the Royal Astronomical Society*, vol. 339, no. 4, pp. 1057–1080, 2003.

[80] I. Zehavi, D. H. Weinberg, Z. Zheng et al., "On departures from a power law in the galaxy correlation function," *Astrophysical Journal Letters*, vol. 608, no. 1, pp. 16–24, 2004.

[81] S. Phleps, J. A. Peacock, K. Meisenheimer, and C. Wolf, "Galaxy clustering from COMBO-17: the halo occupation distribution at z = 0.6," *Astronomy and Astrophysics*, vol. 457, no. 1, pp. 145–155, 2006.

[82] Z. Zheng, I. Zehavi, D. J. Eisenstein, D. H. Weinberg, and Y. P. Jing, "Halo occupation distribution modeling of clustering of luminous red galaxies," *Astrophysical Journal*, vol. 707, no. 1, pp. 554–572, 2009.

[83] J. S. Bullock, R. H. Wechsler, and R. S. Somerville, "Galaxy halo occupation at high redshift," *Monthly Notices of the Royal Astronomical Society*, vol. 329, no. 1, pp. 246–256, 2002.

[84] L. A. Moustakas and R. S. Somerville, "The masses, ancestors, and descendants of extremely red objects: constraints from spatial clustering," *Astrophysical Journal*, vol. 577, no. 1, pp. 1–10, 2002.

[85] T. Hamana, M. Ouchi, K. Shimasaku, I. Kayo, and Y. Suto, "Properties of host haloes of Lyman-break galaxies and Lyman α emitters from their number densities and angular clustering," *Monthly Notices of the Royal Astronomical Society*, vol. 347, no. 3, pp. 813–823, 2004.

[86] Z. Zheng, "Interpreting the observed clustering of red galaxies at z ~ 3," *Astrophysical Journal Letters*, vol. 610, no. 1, pp. 61–68, 2004.

[87] Z. Zheng, A. L. Coil, and I. Zehavi, "Galaxy evolution from halo occupation distribution modeling of DEEP2 and SDSS galaxy clustering," *Astrophysical Journal*, vol. 667, no. 2, pp. 760–779, 2007.

[88] A. V. Kravtsov, A. A. Berlind, R. H. Wechsler et al., "The dark side of the halo occupation distribution," *Astrophysical Journal*, vol. 609, no. 1, pp. 35–49, 2004.

[89] C. Porciani, M. Magliocchetti, and P. Norberg, "Cosmic evolution of quasar clustering: implications for the host haloes," *Monthly Notices of the Royal Astronomical Society*, vol. 355, no. 3, pp. 1010–1030, 2004.

[90] N. Padmanabhan, M. White, P. Norberg, and C. Porciani, "The real-space clustering of luminous red galaxies around z < 0.6 quasars in the Sloan Digital Sky Survey," *Monthly Notices of the Royal Astronomical Society*, vol. 397, no. 4, pp. 1862–1875, 2009.

[91] Y. Shen, J. F. Hennawi, F. Shankar et al., "Binary quasars at high redshift. II. Sub-Mpc clustering at z ∼ 3-4," *Astrophysical Journal Letters*, vol. 719, no. 2, pp. 1693–1698, 2010.

[92] S. Starikova, R. Cool, D. Eisenstein et al., "Constraining halo occupation properties of x-ray active galactic nuclei using clustering of Chandra sources in the Botes survey region," *Astrophysical Journal*, vol. 741, no. 1, article 15, 2011.

[93] T. Miyaji, M. Krumpe, A. L. Coil, and H. Aceves, "The spatial clustering of rosat all-sky survey AGNs. II. halo occupation distribution modeling of the cross-correlation function," *Astrophysical Journal Letters*, vol. 726, no. 2, article 83, 2011.

[94] T. J. Arnold, P. Martini, J. S. Mulchaey, A. Berti, and T. E. Jeltema, "Active galactic nuclei in groups and clusters of galaxies: detection and host morphology," *Astrophysical Journal*, vol. 707, no. 2, pp. 1691–1706, 2009.

[95] P. Martini, G. R. Sivakoff, and J. S. Mulchaey, "The evolution of active galactic nuclei in clusters of galaxies to redshift 1.3," *Astrophysical Journal*, vol. 701, no. 1, pp. 66–85, 2009.

[96] J. D. Silverman, K. Kova, and C. Knobel, "The environments of active galactic nuclei within the zCOSMOS density field," *The Astrophysical Journal*, vol. 695, no. 1, p. 171, 2009.

[97] C. Li, G. Kauffmann, L. Wang, S. D. M. White, T. M. Heckman, and Y. P. Jing, "The clustering of narrow-line AGN in the local Universe," *Monthly Notices of the Royal Astronomical Society*, vol. 373, no. 2, pp. 457–468, 2006.

[98] A. L. Coil, J. F. Hennawi, J. A. Newman, M. C. Cooper, and M. Davis, "The DEEP2 galaxy redshift survey: clustering of quasars and galaxies at z = 1," *Astrophysical Journal Letters*, vol. 654, no. 1, pp. 115–124, 2007.

[99] G. Mountrichas, U. Sawangwit, T. Shanks et al., "QSO-LRG two-point cross-correlation function and redshift-space distortions," *Monthly Notices of the Royal Astronomical Society*, vol. 394, no. 4, pp. 2050–2064, 2009.

[100] R. C. Hickox, A. D. Myers, M. Brodwin et al., "Clustering of obscured and unobscured quasars in the Boötes field: placing rapidly growing black holes in the cosmic web," *Astrophysical Journal Letters*, vol. 731, no. 2, article 117, 2011.

[101] P. Martini and D. H. Weinberg, "Quasar clustering and the lifetime of quasars," *Astrophysical Journal*, vol. 547, no. 1, pp. 12–26, 2001.

[102] A. C. Fabian, R. V. Vasudevan, R. F. Mushotzky, L. M. Winter, and C. S. Reynolds, "Radiation pressure and absorption in AGN: results from a complete unbiased sample from *Swift*," *Monthly Notices of the Royal Astronomical Society*, vol. 394, no. 1, pp. L89–L92, 2009.

[103] P. F. Hopkins, T. J. Cox, D. Kerbš, and L. Hernquist, "A cosmological framework for the co-evolution of Quasars, supermassive black holes, and elliptical galaxies. II. Formation of red ellipticals," *Astrophysical Journal, Supplement Series*, vol. 175, no. 2, pp. 390–422, 2008.

[104] G. Hasinger, "Absorption properties and evolution of active galactic nuclei," *Astronomy and Astrophysics*, vol. 490, no. 3, pp. 905–922, 2008.

[105] Y. Shen, "Supermassive black holes in the hierarchical universe: a general framework and observational tests," *Astrophysical Journal Letters*, vol. 704, no. 1, pp. 89–108, 2009.

[106] F. Shankar, D. H. Weinberg, and J. Miralda-Escudé, "Self-consistent models of the AGN and black hole populations: duty cycles, accretion rates, and the mean radiative efficiency," *Astrophysical Journal*, vol. 690, no. 1, pp. 20–41, 2009.

[107] F. Shankar, C. Martin, M.-E. Jordi, F. Pablo, H. W. David et al., "On the radiative efficiencies, eddington ratios, and duty cycles of luminous high-redshift quasars," *The Astrophysical Journal*, vol. 718, no. 1, article 231, 2010.

[108] F. Shankar, "Merger-induced quasars, their light curves, and their host halos," in *Proceedings of the International Astronomical Union (IAUS '10)*, vol. 267, pp. 248–253, 2010.

[109] E. Treister, C. M. Urry, K. Schawinski, C. N. Cardamone, and D. B. Sanders, "Heavily obscured active galactic nuclei in high-redshift luminous infrared galaxies," *Astrophysical Journal*, vol. 722, no. 2, pp. L238–L243, 2010.

[110] A. Georgakakis, K. Nandra, E. S. Laird et al., "AEGIS: the environment of X-ray sources at z ∼ 1," *Astrophysical Journal Letters*, vol. 660, no. 1, pp. L15–L18, 2007.

[111] A. Georgakakis, A. L. Coil, E. S. Laird et al., "Host galaxy morphologies of X-ray selected AGN: assessing the significance of different black hole fuelling mechanisms to the accretion density of the Universe at z ∼ 1," *Monthly Notices of the Royal Astronomical Society*, vol. 397, no. 2, pp. 623–633, 2009.

[112] M. Cisternas, K. Jahnke, K. J. Inskip et al., "The bulk of the black hole growth since z ∼ 1 occurs in a secular universe: no major merger-AGN connection," *Astrophysical Journal Letters*, vol. 726, no. 2, article 57, 2011.

[113] J. S. Dunlop, R. J. McLure, M. J. Kukula, S. A. Baum, C. P. O'Dea, and D. H. Hughes, "Quasars, their host galaxies and their central black holes," *Monthly Notices of the Royal Astronomical Society*, vol. 340, no. 4, pp. 1095–1135, 2003.

[114] N. A. Grogin, C. J. Conselice, E. Chatzichristou et al., "AGN host galaxies at z ∼ 0.4-1.3: bulge-dominated and lacking merger-AGN connection," *Astrophysical Journal*, vol. 627, no. 2, pp. L97–L100, 2005.

[115] C. M. Pierce, J. M. Lotz, E. S. Laird et al., "AEGIS: host galaxy morphologies of X-ray-selected and infrared-selected active galactic nuclei at 0.2 ≤ z < 1.2," *Astrophysical Journal Letters*, vol. 660, no. 1, pp. L19–L22, 2007.

[116] J. M. Gabor, C. D. Impey, K. Jahnke et al., "Active galactic nucleus host galaxy morphologies in cosmos," *The Astrophysical Journal*, vol. 691, no. 1, article 705, 2009.

[117] T. A. Reichard, T. M. Heckmas, and G. Rudnick, "The lopsidedness of present-day galaxies: connections to the formation of stars, the chemical evolution of galaxies, and the growth of black holes," *The Astrophysical Journal*, vol. 691, no. 2, article 1005, 2009.

[118] T. Tal, P. G. Van Dokkum, J. Nelan, and R. Bezanson, "The frequency of tidal features associated with nearby luminous elliptical galaxies from a statistically complete sample," *Astronomical Journal*, vol. 138, no. 5, pp. 1417–1427, 2009.

[119] D. J. Schlegel, F. Abdalla, and T. Abraham, "The BigBOSS experiment," *Astrophysics*, vol. 1, no. 11, p. 2865, 2011.

[120] D. J. Rosario, R. C. McGurk, and C. E. Max, "Adaptive optics imaging of QSOs with double-peaked narrow lines: are they dual AGNs?" *The Astrophysical Journal*, vol. 739, no. 1, article 44, 2011.

[121] K. Schawinski, M. Urry, E. Treister, B. Simmons, P. Natarajan, and E. Glikman, "Evidence for three accreting black holes in a galaxy at z ∼ 1.35: a snapshot of recently formed black hole seeds?" *Astrophysical Journal Letters*, vol. 743, no. 2, article L37, 2011.

[122] D. D. Kocevski, S. M. Faber, M. Mozena et al., "Candels: constraining the AGN-merger connection with host morphologies at z ∼ 2," *Astrophysical Journal*, vol. 744, no. 2, article 148, 2012.

[123] D. J. Eisenstein, D. H. Weinberg, and E. Agol, "SDSS-III: massive spectroscopic surveys of the distant universe, the milky way galaxy, and extra-solar planetary systems," *The Astronomical Journal*, vol. 142, no. 3, article 72, 2011.

[124] P. Predehl, R. Andritschke, W. Bornemann et al., "eROSITA," in *UV, X-Ray, and Gamma-Ray Space Instrumentation for Astronomy XV*, vol. 6686 of *Proceedings of SPIE*, August 2007.

[125] Z. Ivezic, J. A. Tyson, E. Acosta et al., "LSST: from science drivers to reference design and anticipated data products," *Bulletin of the American Astronomical Society*, vol. 41, p. 366, 2008.

[126] M. Davis and P. J. E. Peebles, "A survey of galaxy redshifts. V—the two-point position and velocity correlations," *Astrophysical Journal*, vol. 267, pp. 465–482, 1983.

[127] K. B. Fisher, M. Davis, M. A. Strauss, A. Yahil, and J. P. Huchra, "Clustering in the 1.2 Jy IRAS galaxy redshift survey II: redshift distortions and $\xi(r_p, \pi)$," *Monthly Notices of the Royal Astronomical Society*, vol. 267, pp. 927–948, 1994.

[128] S. D. Landy and A. S. Szalay, "Bias and variance of angular correlation functions," *Astrophysical Journal*, vol. 412, no. 1, pp. 64–71, 1993.

[129] P. Norberg, C. M. Baugh, E. Gaztañaga, and D. J. Croton, "Statistical analysis of galaxy surveys—I. Robust error estimation for two-point clustering statistics," *Monthly Notices of the Royal Astronomical Society*, vol. 396, no. 1, pp. 19–38, 2009.

[130] C. Blake, A. Collister, and O. Lahav, "Halo-model signatures from 380 000 Sloan Digital Sky Survey luminous red galaxies with photometric redshifts," *Monthly Notices of the Royal Astronomical Society*, vol. 385, no. 3, pp. 1257–1269, 2008.

[131] S. R. Knollmann, C. Power, and A. Knebe, "Dark matter halo profiles in scale-free cosmologies," *Monthly Notices of the Royal Astronomical Society*, vol. 385, no. 2, pp. 545–552, 2008.

[132] J. Stadel, D. Potter, B. Moore et al., "Quantifying the heart of darkness with GHALO—a multibillion particle simulation of a galactic halo," *Monthly Notices of the Royal Astronomical Society*, vol. 398, no. 1, pp. L21–L25, 2009.

[133] D. J. Eisenstein and W. Hu, "Power spectra for cold dark matter and its variants," *Astrophysical Journal Letters*, vol. 511, no. 1, pp. 5–15, 1999.

[134] R. E. Smith, J. A. Peacock, A. Jenkins et al., "Stable clustering, the halo model and non-linear cosmological power spectra," *Monthly Notices of the Royal Astronomical Society*, vol. 341, no. 4, pp. 1311–1332, 2003.